Macromolecules

pubs.acs.org/Macromolecules Perspective

Scaling Perspective on Dynamics of Nanoparticles in Polymers: Length- and Time-Scale Dependent Nanoparticle−Polymer Coupling

Ting Ge*

Cite This: *Macromolecules* 2023, 56, 3809−3837 Read Online

ACCESS | Metrics & More | Article Recommendations

ABSTRACT: The motion of nanoparticles in a polymer matrix is dictated by the intricate coupling of the nanoparticles and surrounding polymers. Various length- and time-scale dependent features of nanoparticle−polymer coupling in a polymer matrix have been delineated in the past decade by combining scaling theory and molecular simulations. Representative scenarios of nanoparticle dynamics in polymers, which embody the roles of polymer matrix topology, the polymers grafted to nanoparticle surface, the anisotropic shape of nanoparticles, and an external driving force, are reviewed. The systems examined demonstrate both the richness of the physics in the nanoparticle−polymer coupling and the capability of the scaling-level description in providing unique insights into the size- and time-dependence of nanoparticle mobility. Following a review of recent work, more scenarios of nanoparticles in polymer matrices, which reflect new pieces of physics in the nanoparticle−polymer coupling, are discussed. Together with the advances in the chemical synthesis of nanoparticles and polymers as well as in the techniques of tracking nanoparticle motion and measuring nanoparticle diffusivity, the microscopic picture of nanoparticle−polymer coupling revealed theoretically and computationally is anticipated to aid in the manipulation of nanoparticles in complex polymeric environments and thus benefit many technological applications.

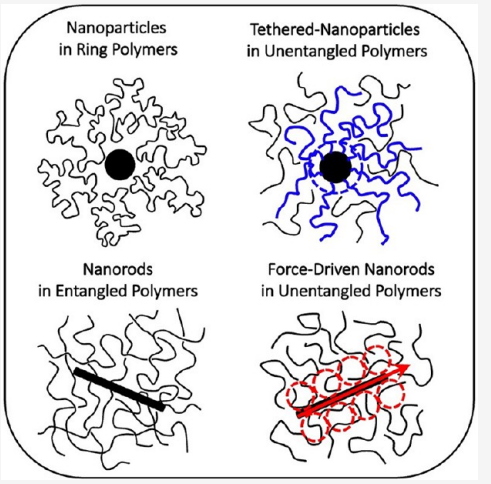

1. INTRODUCTION

The dynamics of nanoparticles in a polymer melt underlie the processing and fabrication of functional nanoparticle polymer composites.[1] The nanoparticle dynamics in viscoelastic polymers also represent a fundamental process in the control of nanoparticles during the particle-based microrheology[2,3] as well as drug and gene delivery in complex polymeric environments.[4−6] The nanoparticle dynamics are determined by the intricate interplay between the nanoparticles and the polymer matrix. In particular, the small size of nanoparticles with respect to the polymers results in the breakdown of the approximation of the polymer matrix as a structureless continuum. Rich features that depend on the length and time scales emerge in the coupling between the nanoparticles and surrounding polymers and manifest themselves in the nanoparticle dynamics.

One starting point to theoretically describe the dynamics of spherical nanoparticles in a polymer matrix is the Stokes−Einstein relation. The diffusion coefficient D, which is defined as the long-time limit of $\langle \Delta r^2(t) \rangle / 6t$, where $\langle \Delta r^2(t) \rangle$ is the mean squared displacement (MSD) of a particle as a function of time t, quantifies the nanoparticle mobility. According to the Einstein relation $D = k_B T/\zeta$, where ζ is the friction coefficient of the particle. Using the Stokes' law, ζ is related to the particle diameter d and the bulk viscosity η as $\zeta = f\eta d$ with the coefficient $f = 2\pi$ or 3π, depending on whether the particle−polymer boundary is full-slip or no-slip.[7] As the bulk viscosity is used in the Stokes−Einstein relation, the result is valid if the polymer matrix may be approximated as a continuum.

The Stokes−Einstein relation was generalized to small length scales where the continuum approximation breaks down by Brochard-Wyart and de Gennes in their seminal 2003 paper on nanoscale viscosity in polymer melts.[8] A length-scale dependent effective viscosity η_{eff} was introduced to replace the bulk melt viscosity η_{melt} in the Stokes−Einstein relation, resulting in $D \approx k_B T/\eta_{eff} d$, where $\approx$ indicates the equation is on the scaling level with the numerical prefactor dropped. The scaling theory describes that η_{eff} is comparable to the viscosity of polymer chain segments whose sizes are comparable to the particle diameter d.

Received: February 13, 2023
Revised: May 5, 2023
Published: May 25, 2023

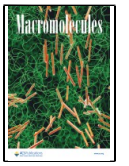

https://doi.org/10.1021/acs.macromol.3c00260
Macromolecules 2023, 56, 3809−3837

Using the Gaussian random-walk statistics, the number of monomers in a chain segment $g \approx d^2/b^2$, where b is the Kuhn monomer size. As a result, the size-dependent effective viscosity is $\eta_{eff} \approx \eta_0 g \approx \eta_0(d^2/b^2)$, where η_0 is the viscosity on the monomer scale. The linear dependence of η_{eff} on g follows the scaling in the Rouse model.[9] The resulting diffusion coefficient is $D \approx k_BT/\eta_0(d^2/b^2)d \sim d^{-3}$, differing from $D \sim d^{-1}$ in the Stokes−Einstein relation. In a melt of short unentangled polymer chains, as d approaches the polymer chain size $R \approx N^{1/2}b$ or equivalently as g approaches the number of monomers N in a melt chain, $\eta_{eff} \approx \eta_{melt} \approx \eta_0 N$ and $D \sim d^{-1}$, which are the results in the continuum theory. However, in a melt of long entangled polymer chains, $\eta_{eff} \approx \eta_{melt}$ and $D \sim d^{-1}$ as d surpasses the entanglement mesh size of the melt $a \approx N_e^{1/2}b$, which is the size of an entanglement strand with $N_e < N$ monomers. The reason for the difference between nanoparticles in unentangled and entangled polymer melts is that the nanoparticles with $d > a$ in entangled polymers are trapped by the entanglement network and have to wait until the relaxation of the entangled polymers to diffuse. The scaling theory by Brochard-Wyart and de Gennes delineates the length-scale dependent coupling between the nanoparticles and polymer melt chains, laying a critical foundation for research on the topic.

The development of nanoparticle chemistry in recent years has enabled the synthesis of nanoparticles with well-controlled size, shape, and surface chemistry, yielding a library of nanoparticles available for investigating fundamental scientific problems and exploring nanoparticle-based applications. Nanoparticles commonly used in the studies of nanoparticle dynamics in a polymer matrix[10−81] include

(1) polyhedral oligomeric silsesquioxanes (POSS) nanoparticles with the diameter d on the order of 1 to 3 nm,[27,40,46]
(2) quantum dots (QDs) with 2 nm < d < 10 nm,[36,67]
(3) gold nanoparticles with 5 nm < d < 400 nm,[11,12,14,19,34,39,43,49,50,55,56,63,78]
(4) magnetic nanoparticles with 5 nm < d < 20 nm,[18,31,37,38,51,52,62,64,70,71,76,80]
(5) silica (SiO_2) nanoparticles with 5 nm < d < 50 nm,[26,29,30,44,48,57,60,61,74,81]
(6) polystyrene nanoparticles with 20 nm < d < 2000 nm,[13,16,17,22,33,35,53,65,66,68,69,72]
(7) nanorods with dimensions from $O(1)$ nm to $O(100)$ nm made of Au, magnetic elements and their dioxides, or titanium dioxide (TiO_2).[15,20,24,45,47,58,79]

Meanwhile, advances in polymer chemistry have prompted the precise synthesis of polymers with well-controlled stereochemistry, monomer sequences, polymer architectures, and molecular interactions, allowing the fabrication of polymer matrices with tunable characteristic length scales and time scales. Apart from the progress in synthetic chemistry, the research on nanoparticle dynamics in a polymer matrix has been propelled by new techniques of tracking the nanoparticles and measuring their diffusivity.[62,82] Various scattering techniques, such as dynamic light scattering (DLS), Rutherford backscattering spectrometry (RBS), X-ray photon correlation spectroscopy (XPCS), and time-of-flight secondary ion mass spectroscopy (ToF-SIMS) can be used to measure the ensemble-averaged diffusivity of nanoparticles. QD-based nanoparticles may be tracked over time to generate trajectories of nanoparticles in a polymer matrix. Additionally, individual nanoparticles may be imaged and tracked in dark field microscopy, fluorescence microscopy, or liquid-phase transmission electron microscopy (TEM). The phenomena in various experiments call for accompanying theoretical and computational studies to promote the understanding of nanoparticle dynamics in polymer matrices.

A scaling perspective on the nanoparticle−polymer coupling in a polymer matrix is provided in this article based on recent work that integrates scaling theory and molecular simulations. The focus is the dynamics of individual nanoparticles in a polymer matrix, which corresponds to a dilute nanoparticle concentration with vanishing interparticle coupling. The effects of nanoparticle interactions, as manifested in the dependence of nanoparticle dynamics on particle concentration in more concentrated systems, are not discussed. Also excluded are the effects of nanoparticles on the dynamics of the polymer matrix as well as on the dynamics and rheology of the polymer nanocomposite as a whole. Readers interested in the excluded topics are advised to read relevant research and review articles.[1,83−86]

This article is organized as follows. Section 2 will review the extension of the scaling theory by Brochard-Wyart and de Gennes[8] to delineate the dynamics of nanoparticles at intermediate time scales prior to the terminal diffusion and the new theory of nanoparticle hopping diffusion in entangled polymer matrices. The brief review is based on the work by Cai, Paniukov, and Rubinstein in the 2010s.[87,88] Section 2 will end with a brief review of the nonscaling theoretical approach developed by Schweizer and his collaborators[89,90] to study nanoparticle dynamics in polymer matrices. Section 3 will briefly describe the models of polymer and nanoparticles in coarse-grained molecular simulations, which are well-positioned to examine scaling relations. Section 4 will summarize recent progress in scaling theory and molecular simulations that broaden the fundamental knowledge of nanoparticle dynamics in a polymer melt. Four representative scenarios are reviewed: (1) the dynamics of nanoparticles in a melt of nonconcatenated ring polymers, which lie at the frontier of polymer physics beyond the conventional linear architecture and exemplify the effects of polymer matrix topology; (2) the dynamics of nanoparticles grafted with polymers, as encountered in the grafted-nanoparticle polymer composites where the grafted layer provides a versatile platform for interfacial molecular engineering; (3) the dynamics of nanorods, which manifests the role of anisotropic particle shape in the coupling between the nanoparticles and polymer melt; and (4) the force-driven dynamics of nanorods, which demonstrates the contrast between the passive thermal motion of particles and active dynamics of driven particles. Each subsection includes a review of relevant experiments and ends with a discussion of related open questions for future research. The article will conclude with Section 5, which further discusses general open questions for future research on nanoparticle−polymer coupling.

2. 2010S' THEORIES OF NANOPARTICLE DYNAMICS IN POLYMERS

2.1. Scaling Theory by Cai, Paniukoiv, and Rubinstein.

To describe the dynamics of nanoparticles on time scales shorter than the terminal diffusion time, Cai, Paniukov, and Rubinstein extended the effective viscosity η_{eff} for the terminal diffusion to a time-dependent effective viscosity $\eta_{eff}(t)$.[87] On the scaling level, a melt of unentangled polymers at a time scale t shorter than the terminal relaxation time τ_{relax} of the melt is equivalent to a melt of chain segments whose relaxation time equals t. The number of

https://doi.org/10.1021/acs.macromol.3c00260
Macromolecules 2023, 56, 3809−3837

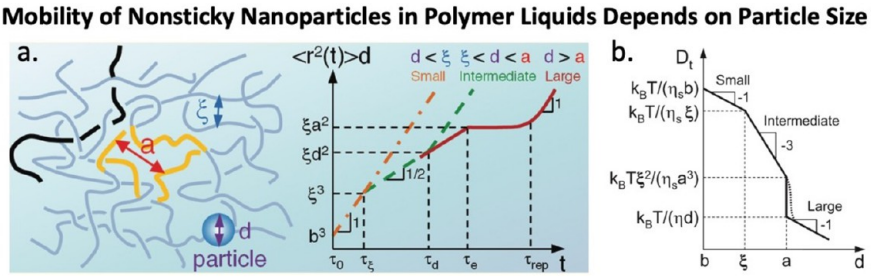

Figure 1. (a) Schematic illustration of a nanoparticle of diameter d in a polymer liquid with indicated characteristic length scales and the d-dependent nanoparticle MSD $\langle \Delta r^2(t) \rangle$. (b) The d-dependence of the terminal diffusion coefficient. Dotted line for d slightly above the entanglement mesh size a indicates the prediction of the hopping diffusion theory [adapted from ref 87].

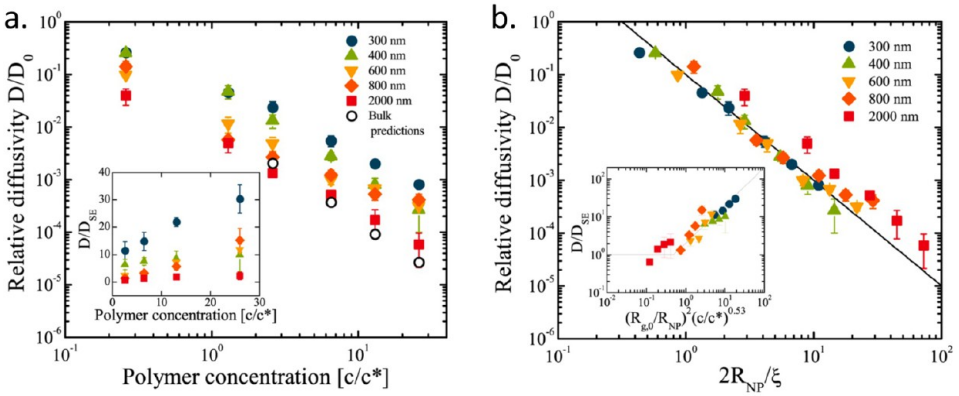

Figure 2. (a) D/D_0, where D and D_0 are the diffusion coefficients of fluorescent polystyrene (PS) nanoparticles of indicated diameter $2R_{NP}$ in the solutions of partially hydrolyzed polyacrylamide (HPAM) and in pure solvents, respectively, as a function of c/c^*, where c and c^* are the solution concentration and the overlap concentration. Inset: D is rescaled by D_{SE}, which is the prediction using the Stokes−Einstein relation with the bulk solution viscosity. (b) D/D_0 plotted against $2R_{NP}/\xi$, where ξ is the correlation length of the polymer solution. The solid line indicates the prediction of the scaling theory by Cai et al. Inset: D/D_{SE} plotted against $(R_{g,0}/R_{NP})^2(c/c^*)^{0.53}$ [adapted from ref 22].

monomers in such a chain segment is $g(t) < N$. According to the Rouse model, the relaxation time of the chain segment is $\tau_g \approx \tau_0 g(t)^2$, where τ_0 is the monomeric time. Equating τ_g and t gives $g(t) \approx (t/\tau_0)^{1/2}$. Therefore, the effective viscosity for the nanoparticle dynamics at time scale t is $\eta_{eff}(t) \approx \eta_0 g(t) \approx \eta_0 (t/\tau_0)^{1/2}$. Generalizing the Stokes' law, Cai et al. then determined that the time-dependent friction coefficient of the particle is $\zeta(t) \approx \eta_{eff}(t) d$. Further use of the Einstein relation results in the time-dependent diffusion coefficient $D(t) = k_B T/\zeta(t)$ and nanoparticle MSD $\langle \Delta r^2(t) \rangle \approx D(t)t \sim t^{1/2}$. The result indicates that the nanoparticle motion is subdiffusive at intermediate time scales, originating from the coupling of the nanoparticle and increasingly longer chain segments with time ($g(t)$ monomers per segment).

The subdiffusive motion eventually ends as the terminal diffusion begins. For d larger than the average polymer chain size R, the crossover to the terminal diffusive regime is at τ_{relax}, as the particles are large enough for the coupling with entire polymer chains. For $d < R$, the crossover is instead at $\tau_d \approx \tau_0 (d/b)^4$, as the particles can at most be coupled with the chain segments of sizes comparable to the particle size d. This d-dependence for the terminal diffusion was already captured in the scaling theory by Brochard-Wyart and de Gennes. Figure 1a shows $\langle \Delta r^2(t) \rangle$ for the nanoparticles of different d with respect to the characteristic length scales of a polymer matrix. The corresponding d-dependence of the terminal diffusion coefficient is shown in Figure 1b. Note that the scaling theory of Cai et al. is for polymer liquids in general. The diffusive motion of nanoparticles of d smaller than the correlation length ξ in a polymer solution is controlled by the solvent viscosity η_s. The results for nanoparticles of $d > \xi$ may be transformed to describe the nanoparticles in polymer melts by replacing ξ with b and η_s with η_0.

The size-dependent dynamics of nanoparticles in unentangled polymers have been confirmed by Poling-Skutvi et al. using polystyrene (PS) nanoparticles with diameter d ranging from 300 to 2000 nm in dilute and semidilute solutions of partially hydrolyzed polyacrylamide (PAM) with the solution concentration c below the entanglement threshold. PS particles were tracked using an inverted microscope and diffusion coefficients D were computed from the one-dimensional ensemble-averaged mean-squared displacement. The particle diffusion coefficients are above the predictions by the Stokes−Einstein relation for the ranges of d and c covered (Figure 2a), though the data points collapse to a universal curve $D \sim (2R_{NP}/\xi)^{-3}$, in agreement with the scaling theory that derives D from the coupling between the particle and the polymer chain segments comparable to the particle in size (Figure 2b).

Cai et al. also described theoretically the crossover from the ballistic motion at a very short time scale to the subdiffusive motion at intermediate time scales. The time scale for the crossover is determined by equating $\langle \Delta r^2(t) \rangle$ for the subdiffusion and $\langle \Delta r^2(t) \rangle_{bal} \approx \langle (v_{thermal} t)^2 \rangle \approx \langle v_{thermal}^2 \rangle t^2$ for the ballistic motion of a nanoparticle with mass m. According to the equipartition theorem, $\langle v_{thermal}^2 \rangle \approx (k_B T)/m$. The time scale at which the ballistic motion ends was found to be $\tau_{bal} \approx \tau_0 (mb^3/\tau_0^2 k_B T d)^{2/3}$. The importance of τ_{bal} is that it sets the lower bound in the time domain for the nanoparticle−polymer coupling.

https://doi.org/10.1021/acs.macromol.3c00260
Macromolecules 2023, 56, 3809−3837

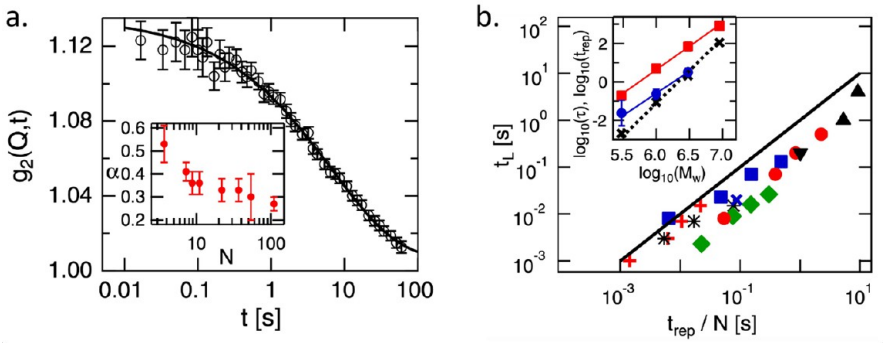

Figure 3. (a) X-ray photon correlation spectroscopy (XPCS) intensity autocorrelation function for polystyrene (PS) solution with molecular weight $M_w = 1 \times 10^6$ g/mol and polymer volume fraction $\phi = 0.3$ containing a dilute concentration of Au nanoparticles at temperature $T = -20°C$ and wave vector $Q = 0.09$ nm^{-1}. The line indicates the best fit to a stretched exponential function with exponent $\alpha = 0.45$ characterizing the subdiffusive nanoparticle motion. Inset: α for Au nanoparticles in different PS solutions as a function of N, which is the number of entanglements per PS chain. (b) Average time t_L for Au nanoparticles to move the entanglement spacing L as a function of t_{rep}/N, where t_{rep} is the reptation time from the rheology experiments of PS solutions. Different symbols correspond to different combinations of M_w and ϕ. Solid line indicates the relation $t_L = 0.3t_{rep}/N$. Inset: mean XPCS relation time τ at $T = 25°C$ and $Q = 0.09$ nm^{-1} for $\phi = 0.3$ (squares) and 0.2 (circles) and t_{rep} at $T = 50°C$ for $\phi = 0.3$ (crosses). Power-law fits give $\tau \sim M_w^{2.4 \pm 0.1}$ and $t_{rep} \sim M_w^{3.2 \pm 0.2}$, as indicated by the solid and dashed lines, respectively [adapted from ref 11].

Nanoparticle motion is ballistic and not affected by the surrounding polymers for $t < \tau_{bal}$.

A major conceptual breakthrough in the theoretical work by Cai et al. is the development of the model of hopping diffusion for a nanoparticle with d moderately larger than the entanglement mesh size a in an entangled polymer melt.[88] Brochard-Wyart and de Gennes argued that a nanoparticle with $d > a$ is trapped by the entanglement network in a polymer melt and must wait until the relaxation of the entangled chains to diffuse. The diffusion time for the nanoparticle diffusion is therefore comparable with the reptation time τ_{rep} of the entangled polymers. Accordingly, MSD is almost constant between the entanglement time τ_e, when entanglements set in, and the reptation time τ_{rep}. Cai et al. instead proposed that the fluctuation of entangled polymer network results in local opening-up of the confinement on nanoparticles, allowing the particles of moderate sizes to diffuse at a time scale shorter than τ_{rep}. They predicted $D \sim \exp(-d/a)$, as indicated by the dotted line in Figure 1b.

The hopping mechanism was employed by Guo et al.[11] to understand the entanglement-controlled subdiffusion of nanoparticles within concentrated polymer solutions. They used X-ray photon correlation spectroscopy (XPCS) to track the motion of Au nanoparticles dispersed at dilute concentrations within the solutions of high-molecular-weight polystyrene (PS). As shown in Figure 3a, the XPCS intensity autocorrelation function fits well to a stretched-exponential function with the stretching exponent $\alpha < 1$ indicating the subdiffusive motion of Au nanoparticles. Further analysis of XPCS and rheology experiment data revealed the average time t_L for nanoparticles to move the entanglement spacing L scales linearly with t_{rep}/N, where t_{rep} and N are the reptation time in the PS solution and the number of entanglements per PS chain, respectively. The relation $t_L \sim t_{rep}/N$ holds for the systems with different PS molecular weights and volume fractions, as shown by the collapse of data points in Figure 3b. Moreover, the mean XPCS relaxation time τ also scales linearly with t_{rep}/N (see inset of Figure 3b). Both $t_L \sim t_{rep}/N$ and $\tau \sim t_{rep}/N$ demonstrated that the mobility of Au nanoparticles is enhanced over polymer diffusion, the rate of which is set by t_{rep} in macroscopic rheology. Guo et al. hypothesized that the subdiffusive motion of nanoparticles in entangled polymer solutions and the enhancement of nanoparticle mobility with respect to the prediction of the macroscopic rheology may be theoretically described with incorporation of the fluctuation-induced hopping mechanism proposed by Cai et al.

2.2. Schweizer's Microscopic Theories. Microscopic theories, which qualitatively differ from scaling theory, have been developed by Schweizer and his collaborators in the 2010s to study the transport of a single nanoparticle in unentangled and entangled polymer melts. Yamamoto and Schweizer[90] identified two competing channels of force relaxation in their microscopic, force-level, self-consistent, generalized Langevin equation approach: the self-motion of the nanoparticle and the length-scale-dependent relaxation of the polymer melt. According to the Yamamoto-Schweizer theory, nanoparticles with diameter d smaller than the entanglement mesh size a exhibit non-Stokes−Einstein long-time diffusivity that is controlled by the fast diffusion and length-scale-dependent collective relaxation of the unentangled chain segments. The long-time diffusivity of nanoparticles with $d > a$, however, is controlled by the reptation of entangled matrix chains. The Yamamoto-Schweizer theory predicted that the two d-dependent regimes are connected by a relatively sharp but continuous crossover and the recovery of the Stokes−Einstein diffusivity requires $d \approx 5-10a$. The predictive power of the Yamamoto-Schweizer theory was demonstrated by the comparisons of the theory with simulations and experiments in the original theory paper[90] as well as by subsequent experiments.[30] While the Yamamoto-Schweizer theory did not include the activated hopping mechanism, in a separate theory developed earlier by Dell and Schweizer[89] using the same microscopic approach, the mechanism of localization and activated hopping of nanoparticles with $d > a$ in entangled polymer melts was formulated. The Dell-Schweizer theory predicted that the hopping diffusivity is much slower with respect to the nanoparticle transport via reptation-driven entanglement network dissolution, except for a narrow window of $d/a \approx 1.5-2$ and sufficiently long melt chains.

3. METHODOLOGY IN NANOPARTICLE−POLYMER SIMULATIONS

Molecular simulations offer a unique tool to investigate the length- and time-scale dependent features of nanoparticle dynamics in a polymer matrix. The spatial and temporal features

https://doi.org/10.1021/acs.macromol.3c00260
Macromolecules 2023, 56, 3809−3837

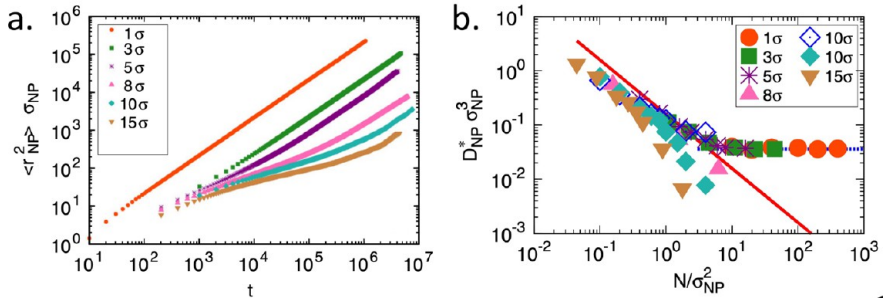

Figure 4. Molecular simulation results: (a) $\langle r_{NP}^2 \rangle \sigma_{NP}$ of nanoparticles with indicated particle diameter σ_{NP} as a function of time t. $\langle r_{NP}^2 \rangle$ is the MSD of the nanoparticles in the polymer melt with chain length $N = 400$. (b) $D_{NP}^* \sigma_{NP}^3$ as a function of N/σ_{NP}^2, where D_{NP}^* is the diffusion coefficient. The red line corresponds to the scaling $D_{NP}^* \sim \sigma_{NP}^{-1}$ in the Stokes−Einstein relation, while the blue dotted line indicates the $D_{NP}^* \sim \sigma_{NP}^{-3}$ when the Stokes−Einstein relation breaks down. Blue open diamonds indicate results from the simulations that allowed polymer chains to cross each other [adapted from ref 100].

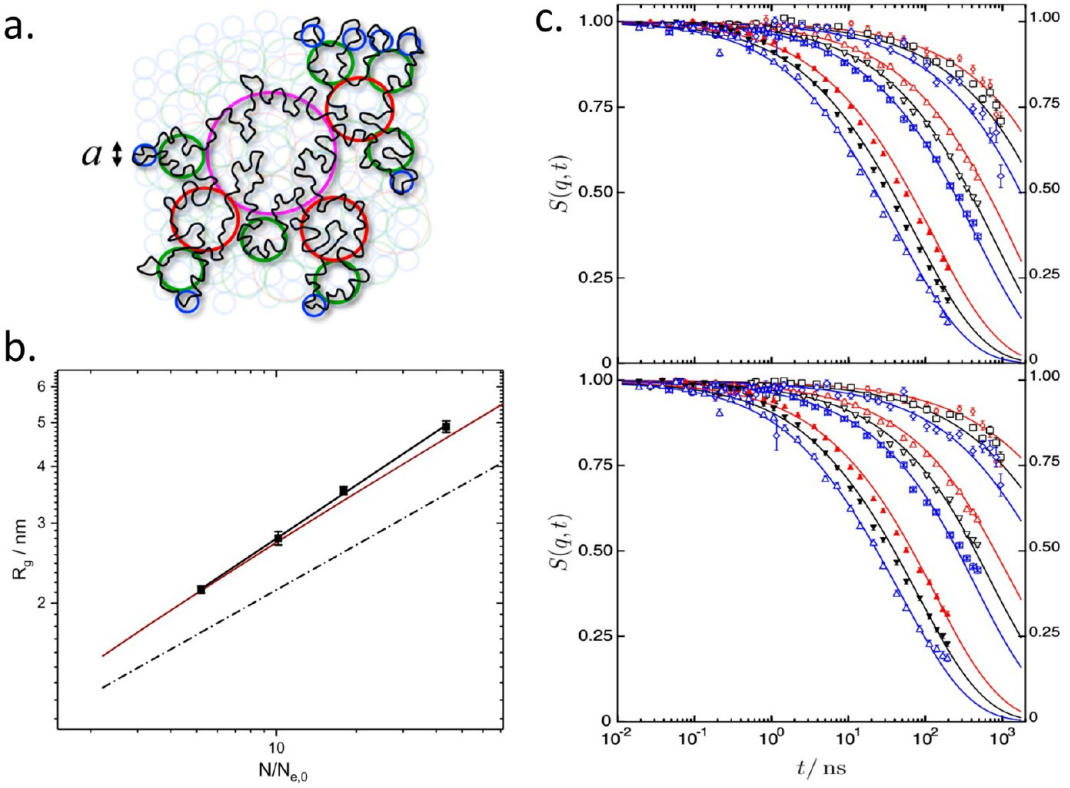

Figure 5. (a) Schematic illustration of the self-similar conformation of a ring polymer in the fractal loopy globule (FLG) model. a is the size of the elementary loop [adapted from ref 123]. (b) Small Angle Neutron Scattering (SANS) result: radius of gyration R_g of polyethylene-oxide (PEO) ring polymers in the melt state as a function of the ring polymer length N rescaled by the elementary loop length $N_{e,0}$. Solid black line indicates the best fit to the power-law function with $R_g \sim (N/N_{e,0})^{0.39}$. Solid red line indicates the result of the decorated loop model by Obukhov et al. Dash dotted line indicates the scaling $R_g \sim (N/N_{e,0})^{1/3}$ in the FLG model [adapted from ref 124]. (c) Neutron Spin Echo (NSE) result: single chain dynamic structure factor $S(q, t)$ for PEO rings with $N/N_{e,0} = 22$ and 44 (upper and lower panels, respectively) at a series of q values from 0.042 Å^{-1} to 0.13 Å^{-1}. Solid lines are the best fit to analytical functions which correspond to $\tau_g \sim (g/N_{e,0})^{2.4}$ for the relaxation of a g-monomer section [adapted from ref 125].

of the coupling between nanoparticles and polymer chains are explicitly constructed in a molecular simulation with direct access to detailed microscopic information, including the positions and momenta of each monomer and nanoparticle. Well-developed open-source simulation packages, such as the Large-scale Atomic/Molecular Massively Parallel Simulator (LAMMPS),[91] are available with active online users' communities providing technical assistance.

The bead−spring polymer model, as in the pioneering work by Kremer and Grest,[92] is a standard model in the molecular simulations of polymers. All beads of size σ and mass m in bead−spring polymers interact via the Lennard-Jones (LJ) potential with unit strength ϵ, a classical force field that captures the hard-core repulsion and the weak intermolecular attraction of the van der Waals type. Neighboring beads in a polymer chain are connected via the finitely extensible nonlinear elastic (FENE) bonding potential, which models the strong covalent backbone of a polymer. Additional bond-bending potential may be added to increase the chain stiffness. A rough mapping of the simulation units to real units is 1 unit length σ to ∼0.5 nm, 1 unit energy ϵ to ∼3 kJ/mol, and 1 unit time $\tau = \sqrt{m\sigma^2/\epsilon}$ to ∼5 ps. Although the bead−spring model is a coarse-grained

https://doi.org/10.1021/acs.macromol.3c00260
Macromolecules 2023, 56, 3809−3837

representation of polymer, it may be mapped to various commodity polymers by varying the bending stiffness to match the experimental values of the Kuhn monomer length, as demonstrated recently by Everaers et al.[93]

A nanoparticle may be simulated directly as a rigid body composed of LJ atoms arranged in a prescribed particle shape.[48,94−97] Alternatively, for spherical and ellipsoidal nanoparticles, the discretized interatomic LJ-potentials may be integrated to yield smooth force fields for both the nanoparticle−nanoparticle and nanoparticle−polymer interactions. A commonly used set of smooth force fields with the Hamaker constant as an explicit model parameter were derived by Everaers and Ejtehadi.[98] With access to a standard high-performance computing cluster nowadays, one can simulate a system containing $O(10^6)$ beads/LJ atoms and $O(10 - 10^2)$ embedded nanoparticles with the particle diameter up to 15σ and generate nanoparticle dynamics trajectories over a period of up to $O(10^6)\tau$. Furthermore, algorithms[99] have been developed to overcome the imbalance of the computing load resulting from the contrasting sizes and cutoff distances of large nanoparticles versus small beads/LJ atoms.

Molecular simulations have been extensively used to study diverse nanoparticle−polymer systems.[48,83,96,97,100−122] Kalathi et al.[100] have systematically performed large-scale molecular simulations of nanoparticle diffusion in linear polymer melts. They obtained the MSDs of nanoparticles and computed the diffusion coefficients D. Their results showed the subdiffusive regime prior to the terminal diffusive regime in MSD (Figure 4a) and confirmed the scaling relation $D \sim d^{-3}$ for the breakdown of the Stokes−Einstein relation in the diffusion of small nanoparticles in polymer melts (Figure 4b). The retarded nanoparticle motion of large nanoparticles in entangled polymers was demonstrated in the MSD and D data. Moreover, by allowing polymer chains to cross each other in the simulations, they observed the absence of the entanglement-induced slowdown in nanoparticle diffusivity, further corroborating the role of polymer entanglements in confining large nanoparticles.

4. RECENT WORK ON NANOPARTICLE−POLYMER COUPLING IN VARIOUS SCENARIOS

4.1. Nanoparticle Dynamics in Ring Polymers—Effects of Polymer Topology. One way to significantly change the structure and dynamics of a polymer matrix is to replace linear polymers with nonconcatenated ring polymers.[126,127] Making the ends of open linear polymer chains meet results in ring polymers with distinctively different conformations and dynamics. The topological constraints of nonconcatenation give rise to the more compact conformations of ring polymers with respect to the Gaussian random-walk coils of linear polymers. The conformation of a ring polymer is captured on the scaling level by the fractal loopy globule (FLG) model.[123] An overview of the FLG ring polymer conformation is given below. The ring conformation is described as a hierarchy of loops in the FLG model, as illustrated in Figure 5a. The smallest loop, termed the elementary loop, consists of N_e monomers. The loops at different length scales overlap with each other at the same overlap parameter O, a quantity defined as the number of overlapping loops that share the same pervaded volume. The overlap parameter in the FLG model is equal to the Kavassalis-Noolandi number $O_{KN} \approx 20$, which is conjectured as the condition for the onset of entanglements in linear polymers.[128] According to the FLG model, the size of a section in a nonconcatenated ring polymer with $g > N_e$ monomers is $r_g^{FLG} \approx (g/N_e)^{1/3}(N_e^{1/2}b)$, which is smaller than $r_g^{RW} \approx g^{1/2}b$ of the Gaussian random-walk coil by a factor of $r_g^{FLG}/r_g^{RW} \approx (N_e/g)^{1/6}$. The overlap parameter $O^{FLG} \approx (r_g^{FLG})^3/(gb^3) \approx N_e^{1/2}$ is constant for $g > N_e$. Beyond the scaling description, Obukhov et al.[129] developed a decorated loop model from assembling polydisperse Gaussian loops in random trees and derived an expression for the deviation from the power-law scaling of the ring polymer radius of gyration, $R_g \sim N^{1/3}$, due to the finite polymer length N.

The topological constraints in nonconcatenated ring polymers do not create a long-lived entanglement network that confines polymers, as the overlap of ring polymers is limited at $O^{FLG} \approx N_e^{1/2}$ for $g > N_e$. Rather the dynamics of nonconcatenated ring polymers with mutual topological constraints are self-similar. In experiments, the self-similar dynamics result in the absence of the rubbery plateau in the stress relaxation modulus $G(t)$, which is a signature of entangled linear polymer rheology.[9] Below, the microscopic picture of the self-similar ring polymer dynamics in the FLG model is briefly described. The topological constraints associated with rearranged smaller loops are effectively released for the dynamics of larger loops in the FLG model. The only effect of the released topological constraints on the larger loops is the increase of the effective friction coefficients of the larger loops. The dynamic release of topological constraints is self-consistent such that at any intermediate time scale, the average spacing between topological constraints is comparable to the characteristic loop that has just been rearranged. On the basis of this microscopic picture, the relaxation time of a g-monomer section in the FLG model is $\tau_g^{FLG} \approx \tau_e(g/N_e)^{7/3}$. It is longer than $\tau_g^{Rouse} \approx \tau_0 g^2 \approx \tau_e(g/N_e)^2$ of a g-monomer section in the Rouse model for unentangled linear polymer dynamics, but shorter than $\tau_g^{Reptation} \approx \tau_e(g/N_e)^3$ of a g-monomer section in the reptation model for entangled linear polymer dynamics. The N-dependence of the melt viscosity $\eta_{melt}^{FLG} \approx \eta_0 N_e(N/N_e)^{4/3}$ in the FLG model is stronger than the linear dependence in $\eta_{melt}^{Rouse} \approx \eta_0 N$ for unentangled linear polymer melts, but weaker than the superlinear dependence in $\eta_{melt}^{Reptation} \approx \eta_0 N_e(N/N_e)^3$ for entangled linear polymers in the reptation model. The new scaling relations τ_g^{FLG} and η_{melt}^{FLG} of nonconcatenated ring polymers distinguish the ring polymers from conventional linear polymers.

The self-similar ring polymer conformations based on elementary loops in the FLG model have been observed in small angle neutron scattering (SANS) experiments on large poly(ethylene oxide) (PEO) rings in the melt by Kruteva et al.[124] The radius of gyration of the PEO rings follows $R_g \sim (N/N_{e,0})^{0.39}$, which may be fit by the expression of the decorated loop model by Obukhov et al.,[129] and yet is comparable to $R_g \sim (N/N_{e,0})^{1/3}$ in the FLG model (Figure 5b). The self-similar relaxation dynamics of the same PEO ring polymers have been confirmed in the neutron spin echo study by Kruteva et al. as well.[125] The FLG model with $\tau_g^{FLG} \approx \tau_e(g/N_e)^{7/3}$ best describes the relaxation of the PEO ring polymers at different length scales, for which the best fit corresponds to $\tau_g \sim (g/N_e)^{2.4}$ (Figure 5c).

Nonconcatenated ring polymers cannot trap embedded nanoparticles with d larger than the average spacing a between the topological constraints, because a long-lived entanglement network is absent in the ring polymer melt. A scaling theory for the coupling between nanoparticles and ring polymers is developed[101] within the theoretical framework constructed by

https://doi.org/10.1021/acs.macromol.3c00260
Macromolecules 2023, 56, 3809−3837

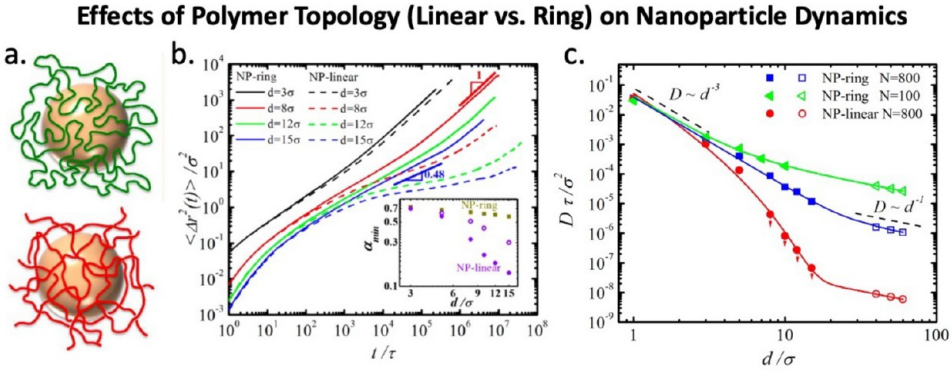

Figure 6. (a) Schematic illustration of a large nanoparticle in nonconcatenated ring polymers (upper) and entangled linear polymers (lower). Molecular simulation results: (b) d-dependent nanoparticle MSD $\langle \Delta r^2(t) \rangle$ and the minimum log−log slope α_{min} and (c) diffusion coefficient D as a function of d for the nanoparticles in the ring and linear polymer melts of indicated length N [adapted from ref 101].

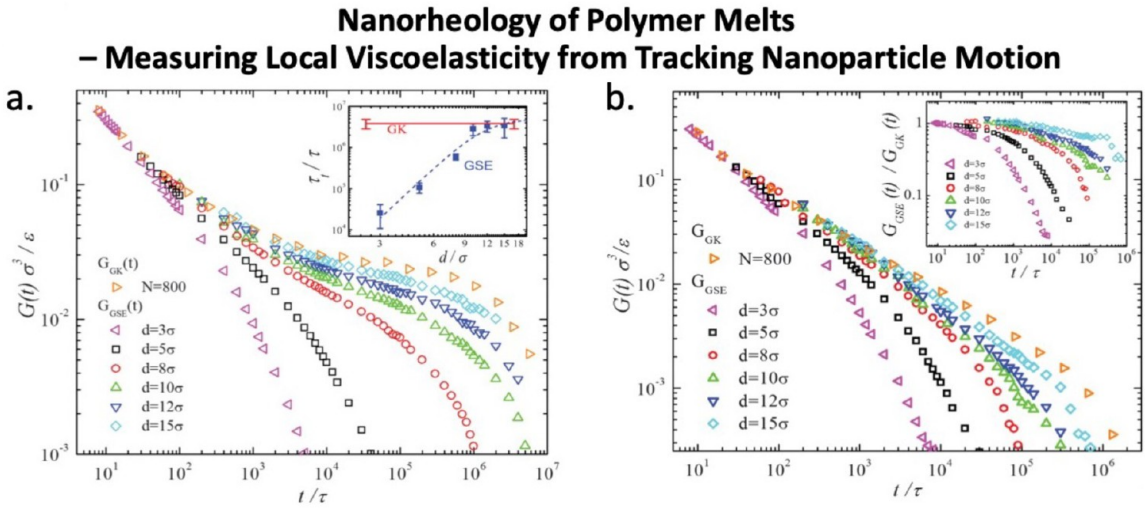

Figure 7. Stress relaxation functions $G_{GK}(t)$ from the Green−Kubo relation for the bulk and $G_{GSE}(t)$ from the generalized Stokes−Einstein relation for the nanoparticle-based rheology in the molecular simulations of nanoparticles in (a) ring polymer and (b) linear polymer melts [adapted from ref 102].

Cai et al.[87,88] Specifically, the effective viscosity $\eta_{eff}(t)$ for nanoparticle dynamics at time scale t is approximated as the bulk viscosity of a melt consisting of g-monomer sections with their relaxation time $\tau_g \approx \tau_e(g/N_e)^{7/3} \approx t$. As a result, $g(t) \approx N_e (t/\tau_e)^{3/7}$ and $\eta_{eff}(t) \approx \eta_0 N_e [g(t)/N_e]^{4/3} \approx \eta_0 N_e (t/\tau_e)^{4/7}$. Further application of the Stokes−Einstein relation results in $D(t) \approx k_B T/\eta_{eff}(t)\ d \sim t^{-4/7}$ and $\langle \Delta r^2(t) \rangle \approx D(t)t \sim t^{3/7}$. As in the nanoparticle dynamics in unentangled linear polymer melts, there is a subdiffusive motion prior to the terminal diffusion, but the scaling exponent for the time dependence is slightly reduced from 1/2 to 3/7. Likewise, for the terminal nanoparticle diffusion, there is a dependence on the particle size d. If d is smaller than the ring polymer size R, the subdiffusive regime ends as the ring sections whose sizes are comparable to d are relaxed. If $d \geq R$, then the subdiffusive regime ends at the terminal relaxation time τ_{relax} of the entire rings.

Molecular dynamics simulations of nanoparticles in linear and ring polymer melts demonstrate the contrasting behaviors of nanoparticle diffusion in the two systems.[101] Subdiffusive motion at intermediate time scales was observed for the nanoparticles in both linear and ring polymer melts, as shown in Figure 6b. The minimum log−log slope of MSD α_{min} decreases with increasing d. For nanoparticles in entangled linear polymers, $\alpha_{min} = 0.14$ for the largest nanoparticles of $d = 15\sigma$, which is about 3 times the entanglement mesh size $a = 5\sigma$. This indicates the trapping of large nanoparticles by the entanglement network. For nanoparticles in the ring polymers, $\alpha_{min} = 0.6$ for $d = 15\sigma$, indicating the absence of an entanglement network that confines nanoparticles. The deviation from the predicted time dependence $\langle \Delta r^2(t) \rangle \sim t^{3/7} \sim t^{0.43}$ based on the FLG model was attributed to the finite-size effects in the simulations. The effects of polymer topology on nanoparticle dynamics were also observed in the d-dependence of the diffusion coefficient D. As shown in Figure 6c, with increasing d, D is strongly suppressed in the entangled polymer melt, while it is less suppressed in the ring polymer melt. Crossover functions guided by the scaling theories for nanoparticles in polymer melts were used to fit the simulation data.

The time-dependent MSDs in the simulations also enabled the investigation of the extension of microrheology to nanorheology.[102] While microrheology relies on colloidal particles with sizes larger than the molecules to explore the bulk viscoelasticity of a medium,[2,3] nanorheology employs nanoparticles with varying sizes to investigate the breakdown of the bulk rheology at the nanoscale. In nanorheology, the conversion of a nanoparticle's MSD to the stress relaxation modulus $G(t)$, which characterizes the rheology of the polymers surrounding the particle, follows the generalized Stokes−Einstein (GSE) relation in microrheology. In the domain of Laplace frequency s, the GSE relation is expressed as $\tilde{G}(s) =$

https://doi.org/10.1021/acs.macromol.3c00260
Macromolecules 2023, 56, 3809−3837

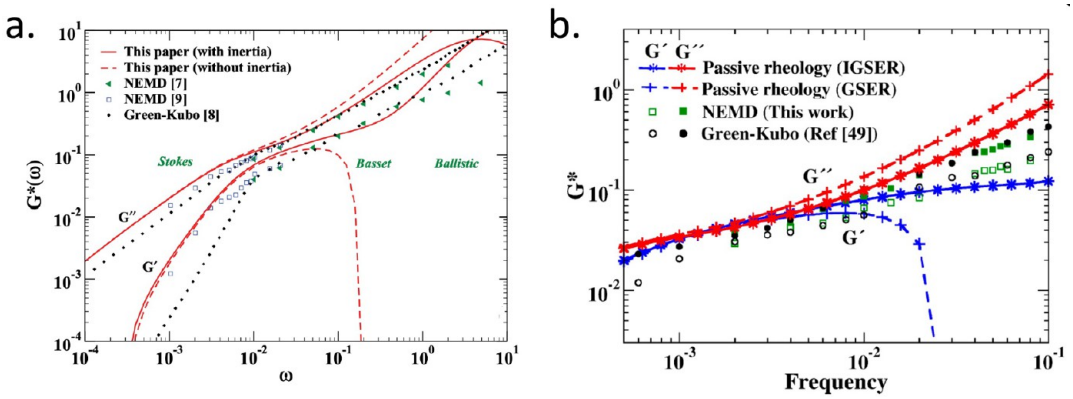

Figure 8. Molecular simulation results: storage modulus G' and loss modulus G'' derived from the MSDs of nanoparticles of radius R in the melt of linear polymer chains of length N. (a) $R = 2.5\sigma$ and $N = 20$ and (b) $R = 12\sigma$ and $N = 80$. Lines are based on the generalized Stokes−Einstein relation with (IGSER) and without the inertia effect (GSER) corrected. Symbols are the bulk rheology data from nonequilibrium molecular dynamics (NEMD) simulations and the Green−Kubo formula [adapted from refs 94,95].

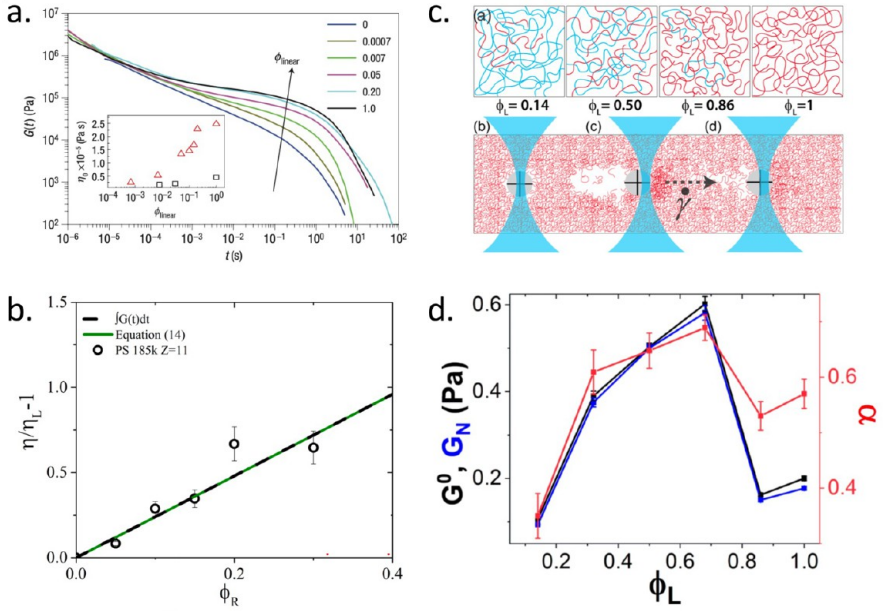

Figure 9. (a) Stress relaxation modulus $G(t)$ for pure polystyrene (PS) ring polymer melt and blends of PS rings and linear chains at indicated linear polymer fraction ϕ_{linear}. Molecular weight is $M_w = 198$ kg/mol for both the ring and linear polymers. Inset: Extrapolated zero-shear-rate viscosity as a function of ϕ_{linear} for $M_w = 198$ kg/mol (triangles) and 160 kg/mol (squares), respectively [adapted from ref 130]. (b) Specific viscosity $\eta/\eta_L - 1$ of a PS ring-linear blend as a function of the ring polymer volume fraction ϕ_R. η and η_L are the zero-shear-rate viscosity of the blend and the pure linear polymer melt, respectively. $M_w = 185$ kg/mol for both the ring and linear polymers in the blends [adapted from ref 131]. (c) Schematic illustration of the blends of entangled ring (blue) and linear (red) DNA of the same contour length at indicated mass fraction ϕ_L of linear DNA and the pulling of a probe particle by an optical tweezer at a constant strain rate $\dot{\gamma}$ in the microrheology experiments. (d) Nonmonotonic dependence of the elastic plateau modulus G^0, the initial relaxation modulus G_N, and shear thinning exponent α on ϕ_L from the linear frequency-dependent microrheology of the ring-linear DNA blends [adapted from ref 132].

$6k_BT/f\pi ds\ \langle \Delta\tilde{r}^2(s)\rangle$, where $\tilde{G}(s)$ and $\Delta\tilde{r}^2(s)$ are the unilateral Laplace transforms of $G(t)$ and $\langle \Delta r^2(t)\rangle$, respectively, and $f = 3$ or 2 depending on whether the particle−polymer boundaries are stick or full slip. The full-slip boundary condition with $f = 2$ was used in the analysis of simulation data, as the particle size was shown to be smaller than the estimated slip length L_s. $\tilde{G}(s)$ was then transformed to $G_{GSE}(t)$ in the time domain and compared with $G_{GK}(t)$, which is the bulk stress relaxation modulus computed using the Green−Kubo formula. A d-dependent deviation of $G_{GSE}(t)$ from $G_{GK}(t)$ was observed, as shown in Figure 7. For nanoparticles in both linear and ring polymers, $G_{GSE}(t)$ approaches $G_{GK}(t)$ with increasing d, but $G_{GSE}(t)$ for the largest d does not completely agree with $G_{GK}(t)$, suggesting that larger d is necessary for the recovery of microrheology.

Karim et al.[94,95] have used molecular simulations to study the effects of inertia on the conversion of nanoparticle MSD to viscoelastic moduli. They simulated nanoparticles in both short unentangled polymers (Figure 8a) and weakly entangled polymers (Figure 8b). The nanoparticle size was sufficiently large to allow the approximation of the polymer melt as a continuum. Both the nanoparticle and medium inertia were shown to affect the applicability of the generalized Stokes−Einstein relation to the simulated systems. The effect of nanoparticle inertia corresponds to the ballistic motion of the nanoparticle on very small time scales or at very high

https://doi.org/10.1021/acs.macromol.3c00260
Macromolecules 2023, 56, 3809−3837

frequencies. The effect of medium inertia arises from the shear elastic wave. It is significant at high frequencies when the elastic wavelength is smaller than the nanoparticle size as well as at very small frequencies when the penetration length of the elastic wave is larger than the spacing between the nanoparticle and its periodic image. Corrections for the inertia effects were proposed to bring the particle-based rheology data to be in a good agreement with the bulk rheology data.

Open Questions. I. One focus in the research field of ring polymers has been the blend of nonconcatenated ring polymers and linear polymers. Starting with resolving the issue of linear polymers as impurities in ring polymers, the study of ring-linear polymer blends has evolved into exploring the volume fraction ϕ_L of linear polymers as an independent control parameter. In a ring-linear polymer blend, the threading of a ring by linear chains emerges as a new topological structure. Rheology experiments and molecular simulations have revealed nonmonotonic dependence of the ring-linear polymer blend viscosity on the blend composition in terms of ϕ_L. Kapnistos et al.[130] studied the effects of linear polymers as the minor component on the stress relaxation and zero shear rate viscosity of ring polymers (Figure 9a). They used polystyrene (PS) melts to demonstrate that linear polymers at a concentration of almost two decades between their overlap cause an enhanced viscosity. Parisi et al.[131] studied stress relaxation and zero shear rate viscosity of symmetric ring-linear PS blends with 30% or less ring component (Figure 9b). Their results demonstrated that both the terminal relaxation time and the viscosity of linear polymers are significantly enhanced by a small fraction of ring polymers. The microscopic mechanisms for composition-dependent rheology are rooted in the events of rings threaded by linear chains. One would expect the dynamics of large nanoparticles in a ring-linear polymer blend to be controlled by the topology of the ring-linear polymer blend, which differs qualitatively from that of a pure polymer melt. As such, an intriguing question for future research is the composition-dependent nanoparticle−polymer coupling in the ring-linear polymer blend. The ring-linear polymer blend also exhibits compositional heterogeneity and thus would serve as a good system to study the effects of heterogeneity on nanoparticle−polymer coupling. Additionally, the threading of rings by linear chains has been recently invoked by Shrestha et al.[69] as a mechanism for the retarded diffusion of soft permeable nanoparticles in entangled polymer melts. A soft nanoparticle consisting of cross-linked polymer chains possesses a fuzzy and loopy surface that may be interpenetrated by the surrounding matrix chains. The state-of-art synthetic schemes have enabled the control of both the soft nanoparticle size and morphology.[133−135] The topological interactions at soft-nanoparticle−polymer interface makes the composite of soft nanoparticles and polymers an emerging system critically controlled by polymer topology. Systems consisting of inorganic nanorings[136,137] in linear polymer chains may be potentially designed as well to further study the role of ring-linear threading in nanoparticle−polymer coupling.

II. The role of polymer chain stiffness in nanoparticle−polymer coupling also needs more systematic studies. Semiflexible polymers, whose dimensions are not significantly larger than the persistence length, exhibit distinctive dynamics modes and rheological features that originate from the bending elasticity.[138] The coupling between nanoparticles and bending-elasticity-dominated dynamics has not been explored much using theory. Elucidation of this piece of new coupling physics has strong motivations from experiments, many of which involve biomacromolecules. Semiflexible actin filaments and rigid microtubules comprise the cytoskeleton, which is a key player in many processes such as vesicle transport, gene delivery, and viral infection. Anderson et al.[139] coupled single-particle tracking with differential dynamic microscopy to characterize the dynamics of microspheres in vitro networks with varying compositions of actin and microtubules. The experiments revealed anomalous subdiffusion of the tracer spheres and its correlation with the competition between network mesh size and filament rigidity. Sonn-Segev et al.[140] used microrheology to study the viscoelastic response of a network of actin filaments at intermediate distances. They found that the length scale above which bulk viscoelasticity sets in the network may appear at a surprisingly large distance and accordingly the local viscoelastic properties of the network persist over length scales much larger than the correlation length and the probe particle size. DNA molecules with intrinsic bending stiffness, another type of biomacromolecules, have been used in both bulk rheology and particle-based microrheology experiments to demonstrate the contrasting effects of linear and cyclic topology. Peddireddy et al.[132] have used optical tweezer microrheology to measure the viscoelastic response of solution blends of entangled ring and linear DNA at varying fractions of linear DNA ϕ_L (Figure 9c). Their results revealed a nonmonotonic dependence of viscoelastic properties, such as the elastic plateau modulus and initial relaxation modulus in linear viscoelasticity and the shear thinning exponent in nonlinear viscoelasticity, on ϕ_L (Figure 9d). Moreover, recent experiments and accompanying simulations have revealed the effects of polymer chain stiffness on the rheological response of nonconcatenated ring polymers.[141] Motivated by these emerging observations in the literature, one future research topic would be adding chain stiffness as another variable to the topology-dependent nanoparticle−polymer coupling. On the simulation side, Chen et al.[54] performed multiparticle collision dynamics simulations of solutions of semiflexible polymers. As chain stiffness increases, the long-time nanoparticle diffusivity in the simulations deviates more from the Stokes−Einstein result D_{SE} and starts to differ from the theoretical prediction of Cai et al.,[87] which was developed for fully flexible polymer chains.

III. Apart from ring polymers, advances in polymer chemistry have enabled the synthesis of polymers with other nonlinear architectures. One prominent system of intensive studies in recent years has been bottlebrush polymer with side chains grafted to a linear polymer backbone.[142−144] Bottlebrush polymers in a melt of chemically identical linear polymers can be directly visualized using super-resolution optical microscopy, as demonstrated by Chan et al.[144] The conformations and dynamics of bottlebrush polymers depend on the side chain length and the grafting density of side chains. In particular, densely grafted side chains make it hard for neighboring bottlebrush polymers to overlap and therefore prevent the formation of an entanglement network. Cai et al.[142] have created Poly(dimethylsiloxane) (PDMS) elastomers from cross-linking the entanglement-free bottlebrushs made of PDMS. The novel PDMS elastomers possess a much reduced shear modulus compared to the conventional PDMS elastomers. The coupling between nanoparticles and bottlebrush polymers would be another new research topic for the role of polymer matrix topology in nanoparticle−polymer coupling. System parameters such as the side chain length and grafting density of side chains are anticipated to endow the nanoparticle−polymer coupling with more topology-related tunability.

https://doi.org/10.1021/acs.macromol.3c00260
Macromolecules 2023, 56, 3809−3837

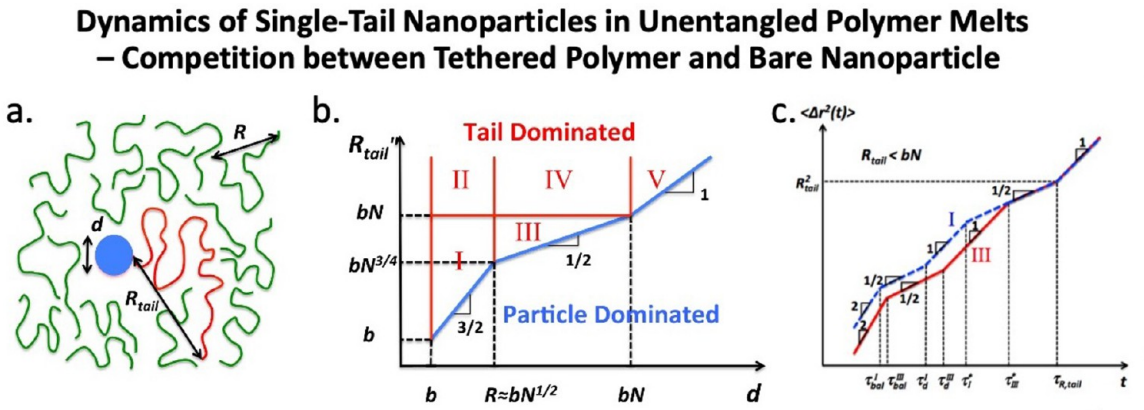

Figure 10. (a) Schematic illustration of a single-tail nanoparticle in an unentangled polymer melt. (b) Diagram indicating the particle-dominated and tail-dominated regimes in the parameter space (d, R_{tail}). (c) MSD $\langle \Delta r^2(t) \rangle$ of single-tail nanoparticles for Regimes I and III in (b) [adapted from ref 147].

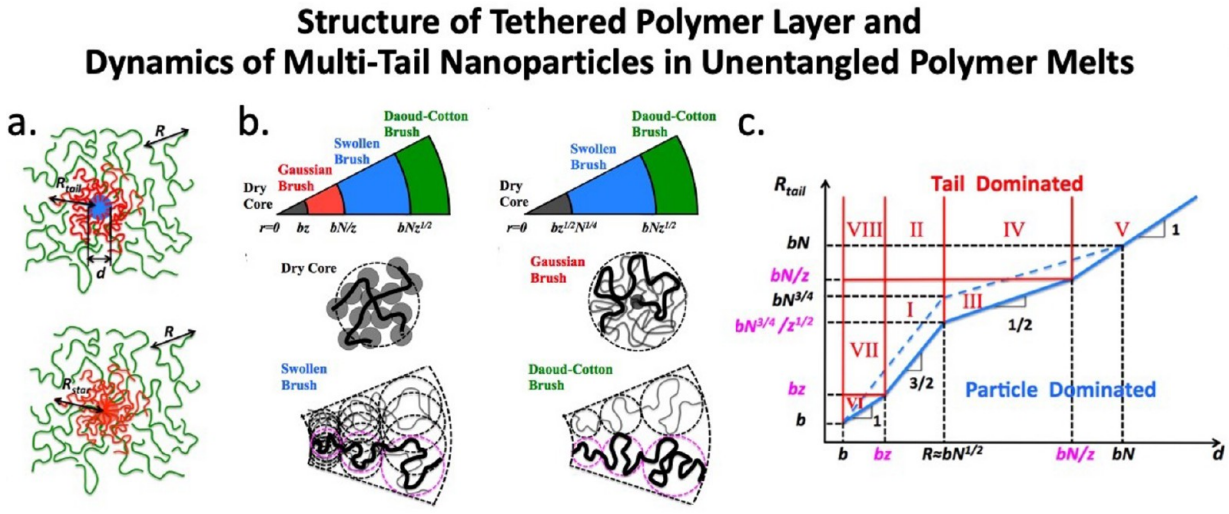

Figure 11. (Schematic illustration of (a) a multitail nanoparticle in an unentangled polymer melt (upper) and the mapping to a multiarm star polymer (lower) and (b) the structure of the multiarm star polymer as a function of the radial distance r from the branching point. (c) Diagram indicating the particle-dominated and tail-dominated regimes of loosely grafted multitail nanoparticles in the parameter space (d, R_{tail}) [adapted from ref 147].

4.2. Dynamics of Polymer-Tethered Nanoparticles—Effects of Tethered Polymer Layer. Polymers are often tethered to nanoparticle surfaces to prevent the aggregation of bare nanoparticles and promote the dispersion of the nanoparticles in a polymer matrix. The grafted polymer layer also provides a platform for the interfacial engineering of nanoparticle polymer composites.[145,146] The tools in synthetic chemistry have enabled precise control of the grafting density, the grafted polymer chain length, and the composition of the grafted layer. Understanding the effects of tethered polymer chains on the diffusion of nanoparticles in a polymer matrix is important to the control of nanoparticles in the nanocomposites. A model system of polymer-tethered nanoparticles in a polymer matrix has been studied using scaling theory.[147] In the model system, the grafted polymers and matrix polymers are chemically identical, and the matrix is a melt of short polymer chains with no entanglements. The scaling analysis demonstrated that the role of tethered polymers in the diffusion of tethered nanoparticles depends on the grafting density and the grafted chain length.

The scaling analysis of the model system started with the ideal scenario where only one polymer chain or tail is grafted to the nanoparticle. The single-tail nanoparticle with the number of tails per particle $Z = 1$ is experimentally challenging but is theoretically simplest and embodies the essential physics. The competition between the friction coefficient ζ_{tail} of the tail and ζ_{bare} of the bare nanoparticle determines whether the terminal diffusion is dominated by the tail with $\zeta_{tail} > \zeta_{bare}$ or the nanoparticle with $\zeta_{tail} < \zeta_{bare}$. If the tail size R_{tail} is smaller than Nb, the melt chains of length N screen the hydrodynamic coupling between distant sections of the tail. Therefore, $\zeta_{tail} \approx \zeta_0 N_{tail} \approx \zeta_0 (R_{tail}/b)^2$, following the Rouse model with the draining of "solvent" molecules. If R_{tail} is larger than Nb, distant sections of size Nb in the tail are hydrodynamically coupled, and $\zeta_{tail} \approx \zeta_0 N^2 (R_{tail}/Nb)$ with no draining of "solvent" molecules as in the Zimm dynamics model. The d-dependent ζ_{bare} of the bare nanoparticle in an unentangled polymer melt is used to describe the friction coefficient of the particle part of the single-tail nanoparticle. As shown in Figure 10b, a detailed comparison of ζ_{tail} and ζ_{bare} determines the boundary between the particle-dominated and the tail-dominated regime in the parameter space (d, R_{tail}), where d and R_{tail} control the corresponding friction coefficients ζ_{bare} and ζ_{tail}, respectively.

https://doi.org/10.1021/acs.macromol.3c00260
Macromolecules 2023, 56, 3809−3837

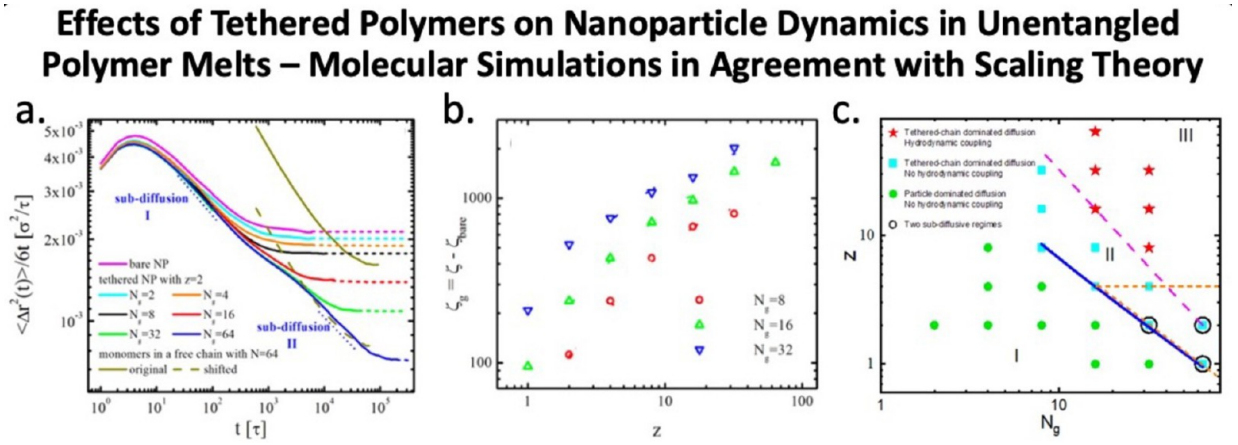

Figure 12. Molecular simulations demonstrating (a) the effect of tethered chain length N_g on the MSD $\langle \Delta r^2(t) \rangle$ of a nanoparticle tethered with $z = 2$ tails and (b) the effects of N_g and z on the nanoparticle friction coefficient ζ. (c) Diagram indicating different regimes of simulated multitail nanoparticles in the parameter space (N_g, z) [adapted from ref 103].

The analysis was further extended to describe the dynamics of tethered nanoparticles prior to the terminal diffusive regime. At times scale t, $\zeta_{bare}(t)$ is compared with $\zeta_{tail}(t)$ to determine whether the dynamics are dominated by the particle or the tail. This comparison is equivalent to the comparison of the bare nanoparticle MSD $\langle \Delta r^2(t) \rangle_{bare}$ and the MSD of monomers in a free tail $\langle \Delta r^2(t) \rangle_{tail}$. On the basis of the result from the comparison, the tail-dominated regime is further divided into different subregimes as indicated by the Roman numerals in Figure 10b. What differs between various tail-dominated regimes is the scaling relation for the crossover time τ^* that separates the tail-dominated motion at time scales $t > \tau^*$ from the particle-dominated motion at time scales $t < \tau^*$. In all tail-dominated subregimes, one prominent feature is the emergence of two subdiffusive regimes in the time-dependent MSD of tethered nanoparticles $\langle \Delta r^2(t) \rangle$. $\langle \Delta r^2(t) \rangle$ of the single-tail nanoparticles in Regimes I and III are sketched in Figure 10c. The first subdiffusive regime lies in the time range of $t < \tau^*$, where $\langle \Delta r^2(t) \rangle \approx \langle \Delta r^2(t) \rangle_{bare}$. It is identical to the subdiffusive motion of bare nanoparticles and arises from the progressive coupling of the particle and polymer chain dynamics. The second subdiffusive regime emerges as $\langle \Delta r^2(t) \rangle \approx \langle \Delta r^2(t) \rangle_{tail}$ in the time range of $t > \tau^*$. It is due to the participation of the nanoparticle in the dynamics of the tail, representing a unique dynamic mode of the particle dragged by the slower-moving tail.

For multitail nanoparticles in an unentangled polymer melt, the scaling theories for multiarm star polymers in a polymer melt[148−151] were employed to describe the structure of the tethered polymers. The structural features of the tethered layer depend on the radial distance r from the particle center. Two distinctive cases were identified.

(1) Loosely branched stars with the number of arms in the range $1 < z_{arm} < N^{1/2}$. Consider sufficiently long arms, for which all r-dependent regions of a star polymer exist. As schematically shown in Figure 11b, the region closest to the branching point is a dense core, where geometric constraints result in densely packed monomers of the star arms, excluding the monomers of the melt chains. Outside the dense core lies the Gaussian brush layer, where chain sections are in the unperturbed Gaussian random-walk conformations with excluded volume interactions screened. With increasing r, excluded volume interactions between different arms emerge and extend the arms with respect to the Gaussian random-walk conformations. A further analysis distinguished the swollen brush layer and the Daoud-Cotton brush.[148]

(2) Densely branched stars with $z_{arm} > N^{1/2}$. For a densely branched star polymer, the Gaussian brush layer is absent, reflecting stronger excluded volume interactions at the same r.

Using the same criterion that determines whether a star polymer is loosely or densely branched in a polymer melt, a multitail nanoparticle in a polymer melt is identified as being either loosely or densely grafted.

(1) Loosely grafted nanoparticles with $1 < z < N^{1/2}$. A diagram showing different scaling regimes in the (d, R_{tail}) parameter space was constructed for loosely grafted nanoparticles, as shown in Figure 11c. Regimes I−V correspond to their counterparts in Figure 10b for single-tail nanoparticles. For Regimes I and III, their boundaries with the particle dominated regime are determined by comparing ζ_{bare} and $z\zeta_{tail}$, as the corresponding multitail nanoparticles may be mapped to the star with a Gaussian brush, where the friction coefficients of individual Gaussian chains are additive with no hydrodynamic coupling among them. For regimes II, IV, and V, the multitail nanoparticles may be mapped to the star with additional non-Gaussian brush layers, where stretched polymer chains are hydrodynamically coupled with each other. The hydrodynamic radius of the multitail NPs may be approximated as the sum of R_{tail} and $d/2$, which is dominated by R_{tail}, as $R_{tail} > d$. Apart from Regimes I−V, new Regimes VI−VIII emerge in Figure 11c. These regimes involve a dry layer outside the bare nanoparticle, corresponding to the dry core of a star polymer.

(2) For densely grafted nanoparticles with $z > N^{1/2}$, no Gaussian brush can exist. As a result, a densely grafted nanoparticle is either mapped to a dry star when the grafted tails are short or a dry core plus hydrodynamically coupled hairy tails when the tails are long enough. In the latter case, the effective hydrodynamic radius is approximated as $R_{tail}+d/2$.

Molecular simulations have been applied to reveal the features of tethered-nanoparticle motion in an unentangled polymer melt and evaluate the scaling theory.[103] In one set of simulations,

https://doi.org/10.1021/acs.macromol.3c00260
Macromolecules 2023, 56, 3809−3837

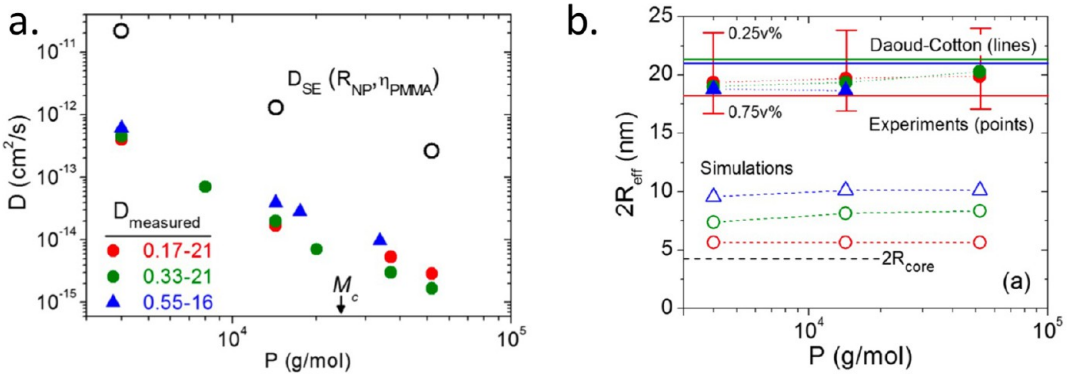

Figure 13. Rutherford backscattering spectrometry results for the diffusion of poly(methyl methacrylate) (PMMA)-grafted iron oxide nanoparticles into a PMMA matrix: (a) the extracted diffusion coefficient D as a function of the matrix molecular weight P for three sample labeled in the format $\Sigma - M$, where Σ is the number of grafted chains per nm^2 and M is the molecular weight of a grafted chain in the unit kg/mol. Open symbols indicate the predictions of the Stokes−Einstein relation D_{SE} using the bare nanoparticle radius R_{NP} and matrix viscosity η_{PMMA}. (b) Effective nanoparticle diameter as determined by the diffusion experiments (solid symbols), the predictions of the modified Daoud-Cotton brush model (solid lines), and the results from dynamic mean field simulations (open symbols) versus P [adapted from ref 38].

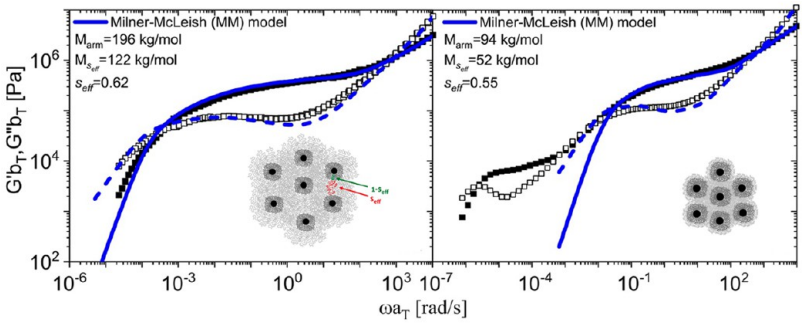

Figure 14. Storage modulus $G'(\omega)$ and loss modulus $G''(\omega)$ of the matrix-free melts of poly(methyl acrylate)-grafted silica (PMA-SiO$_2$) nanoparticles with indicated molecular weight per tethered arm M_{arm}. Symbols are the results of linear rheology experiments. Lines are the best fits to the Milner−McLeish model, in which the fraction of monomers participate in the arm retraction is S_{eff} [adapted from ref 152].

a nanoparticle has $z = 2$ grafted tails, corresponding to a nanoparticle attached to the center of a twice longer chain. As shown in Figure 12a, with increasing grafted chain length N_g, the terminal diffusion coefficient $D = \lim_{t\to\infty} \langle \Delta r^2(t) \rangle / 6t$ decreases, exhibiting the predicted crossover from the particle-dominated to the tail-dominated diffusion. For the longest $N_g = 64$, the MSD of the grafted nanoparticle is comparable to the MSD of monomers in the free chain divided by $z = 2$. However, the two are not identical, reflecting effects not captured by the scaling description. The two subdiffusive regimes predicted for the tail-dominated regime were also observed in the simulations. $\langle \Delta r^2(t) \rangle$ in the two subdiffusive regimes are comparable to the bare NP MSD $\langle \Delta r^2(t) \rangle_{bare}$ and $\langle \Delta r^2(t) \rangle_{tail}/2$, respectively, indicating the respective origins of the two subdiffusive regimes.

In other sets of simulations,[103] the tethered chain length N_g was fixed at the melt chain length N, while the number of tethered chains per particle z was systematically increased. $\zeta_g \approx \zeta - \zeta_{bare}$ is plotted as a function of z in Figure 12b. The initial linear increase of ζ_g means that the friction coefficients of z individual tails are additive and thus $\zeta_g \sim z$. The deviation from the linear z-dependence with increasing z demonstrates the reduction in ζ due to the hydrodynamic coupling between the tethered polymers. Figure 12c is a diagram in the (z, N_g) parameter space that illustrates three qualitative different regimes in the simulations, which differ in whether the diffusion is dominated by the particle or the tails and whether there is hydrodynamic coupling between the multiple tails. The region with two subdiffusive regimes in the MSD plot is indicated in the parameter space as well.

Experiments on tethered nanoparticles in polymers have focused on the densely grafted case. Lin et al.[38] used Rutherford backscattering spectrometry to measure the diffusion coefficient D of PMMA-grafted iron-oxide nanoparticles in unentangled to slightly entangled PMMA melts and found that D is smaller than the prediction of the Stokes−Einstein relation by up to 2 orders of magnitude (Figure 13a). The effective nanoparticle size determined by the Stokes−Einstein relation with the bulk melt viscosity $2R_{eff}$ is approximately the bare nanoparticle size plus the size of the grafted chains, as in the Daoud-Cotton brush model (Figure 13b). Lin et al. also performed dynamic mean field simulations and showed that R_{eff} is larger than the radial distance at which the volume fractions of grafted and matrix polymers are comparable. These results agree with the prediction of the scaling theory[147] that the effective hydrodynamic radius of densely grafted nanoparticles in polymer melts are comparable with $R_{tail} + d/2$.

Open Questions. I. The research on tethered-nanoparticle−polymer coupling may be extended to study nanoparticles tethered with long tails that can get entangled with the entanglement network in a melt of long polymer chains. One motivation for designing such a composite system is the mechanical interlocking of the nanoparticles and polymer matrix promoted by the entanglements between the tethered chains and matrix chains. The simplest scenario of a nanoparticle with d

https://doi.org/10.1021/acs.macromol.3c00260
Macromolecules 2023, 56, 3809−3837

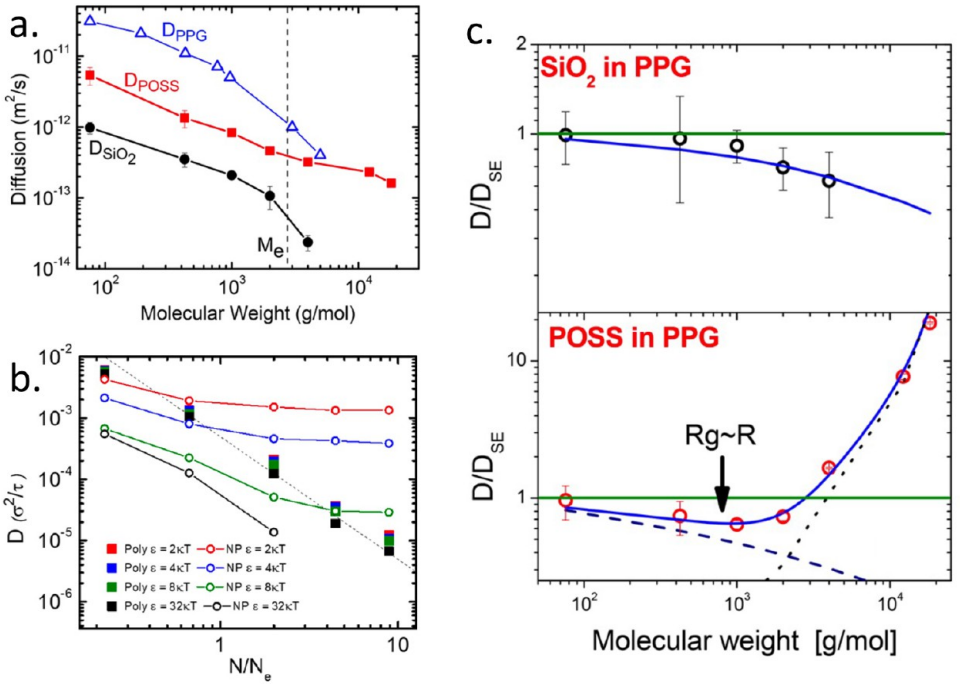

Figure 15. (a) Diffusion coefficients D of silica (SiO_2) nanoparticles, octaamino-phenylsilsesquioxane (OAPS) nanoparticles, and polypropylene glycol (PPG) chains in PPG melts as functions of the molecular weight M_w of PPG melt chains. D of the nanoparticles were obtained using Dynamic Light Scattering (DLS). Dashed line indicates the entanglement molecular weight M_e. (b) Molecular simulation result: D of small sticky nanoparticles, which were modeled as icosahedrons composed of 12 LJ beads of diameter σ, and polymer chains in the polymer melts of chain length N as functions of N/N_e. $N_e = 45$ is the entanglement length. ϵ is the strength of the interaction between a LJ bead in a nanoparticle and a monomer. (c) D/D_{SE} vs M_w for the SiO_2 and POSS nanoparticles in the PPG melts. D_{SE} is the prediction of the Stokes−Einstein relation. For SiO_2, the blue solid line indicates the prediction of the core−shell model. For POSS, the blue solid line indicates the predicted crossover from the core−shell to the vehicular diffusion mechanism [adapted from ref 48].

$< a$ and $z = 1$ or 2 tails may be described by considering the competition between the bare particle dynamics and the reptation dynamics of a long polymer chain in the entanglement network. The more complicated scenarios of nanoparticles with $z \geq 3$ tails may be mapped to star polymers in an entanglement network, where arm retraction emerges as a new mode of dynamics. Existing microscopic theories for the dynamics of entangled star polymer melts may be employed to develop the theoretical description of the dynamics of nanoparticles with multiple entangled tails. Recently, Parisi et al.[152] have studied the linear viscoelasticity of the matrix-free melt of polymer-tethered nanoparticles and observed the arm retraction in the dynamics of sufficiently long tethered chains, which can be described using the Milner−McLeish model of entangled star polymers (Figure 14a). As the length of tethered chains is reduced, there is a crossover to the jammed colloidal system (Figure 14b). For tethered nanoparticles dispersed in an entangled polymer melt, one topic for future research is the emergence of arm retraction with increasing grafted chain length N_g and its effects on the particle dynamics.

II. Intermediate between a bare nanoparticle with only weak nanoparticle−polymer interactions and a tethered nanoparticle with a permanently grafted polymer layer is a sticky nanoparticle to which matrix polymer chains can adsorb. Research on the dynamics of sticky nanoparticles in a polymer matrix will guide the use of surface chemistry tools to tune the attractive strength or stickiness between the nanoparticles and polymers and thus enable better control of nanoparticles in the composites. A recent theory by Yamamoto and Schweizer[153] predicted a transition from "core-shell" diffusion, where the nanoparticle core and the shell of adsorbed polymers diffuse as a combined hydrodynamic object, to "vehicular" diffusion, where the nanoparticle uses the adsorption layer as a "vehicle" to diffuse over a characteristic desorption time scale. They also predicted that the transition occurs as the matrix chain size exceeds the nanoparticle size. Molecular simulations and experiments of sticky nanoparticle diffusion have been performed and interpreted using the "core-shell"-to-"vehicular" diffusion mechanism.[48,153,154] One example of integrated theory-simulation-experiment work[48] is shown in Figure 15, where the diffusion of OAPS nanoparticles in PPG melts was measured using Dynamic Light Scattering. In another experiment by Bailey et al.,[154] Rutherford backscattering spectrometry was used to measure the diffusion of OAPS nanoparticles in poly(2-vinylpridine) (P2VP) melts. The OAPS diffusion coefficients were found to scale very weakly with the molecular weight of P2VP chains, and the OAPS diffusion rate was determined to be at time scales intermediate between the Rouse times of a Kuhn monomer and an entanglement strand. The experiment results were also interpreted using the "vehicle" diffusion mechanism. Additional molecular simulations and experiments with an expanded scan of the parameter space may further evaluate the proposed diffusion mechanisms for sticky nanoparticles. An alternative theoretical description of sticky nanoparticle dynamics may be developed based on the approximation of the adsorption layer as an effective tethered polymer layer whose lifetime is controlled by the adsorption strength and the matrix chain length.[155] Indeed, there are experiments consistent with this approximation. Park et al.[67] used quantum dots (QDs) to perform single-particle tracking of nanoparticles in unentangled

https://doi.org/10.1021/acs.macromol.3c00260
Macromolecules 2023, 56, 3809−3837

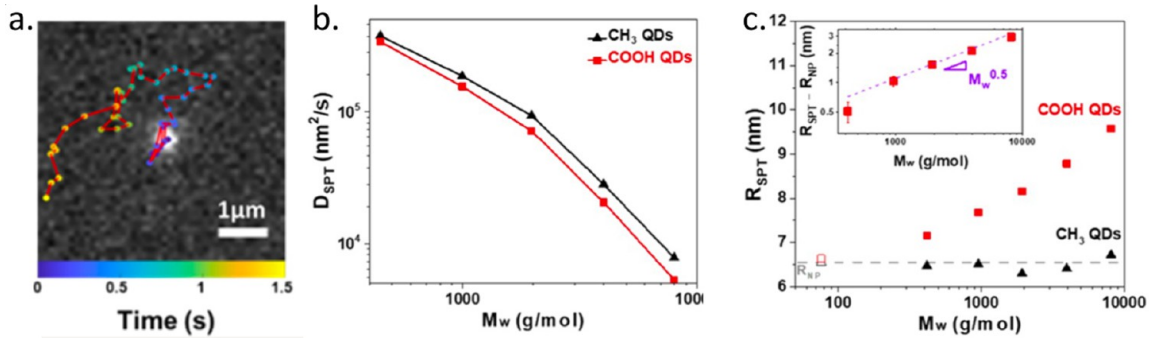

Figure 16. ((a) Trajectory of a single nanoparticle made of a quantum dot (QD) in an unentangled polymer melt. (b) Diffusion coefficient D_{SPT} from the single-particle tracking of nonsticky CH_3-capped and sticky COOH-capped QDs in unentangled melts of poly(propylene glycol) (PPG) vs PPG molecular weight M_w. (c) Apparent QD size R_{SPT}, which is calculated using the Stokes−Einstein relation, vs M_w. Inset shows the enlargement of R_{SPT} with respect to the bare nanoparticle size R_{NP} for the sticky QDs [adapted from ref 67].

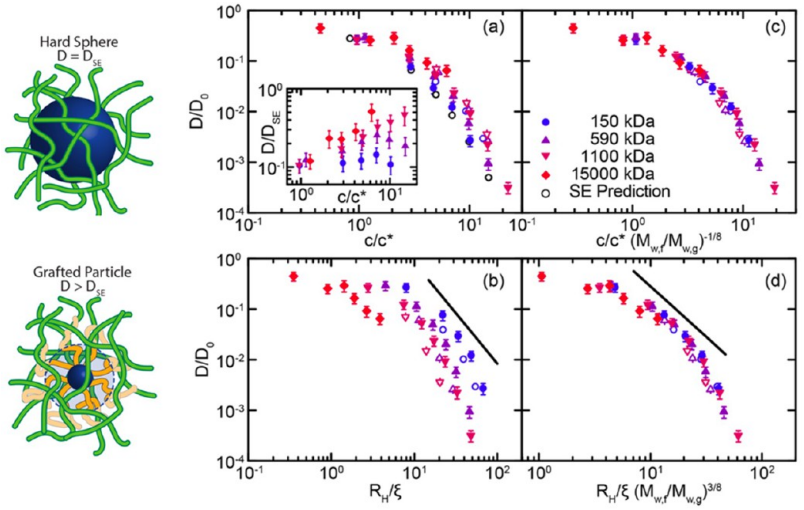

Figure 17. X-ray photon correlation spectroscopy results: (a) D/D_0, where D and D_0 are the diffusion coefficients of polystyrene grafted silica (PS-SiO_2) nanoparticles dispersed in the solution of protonated solvent and PS and in pure solvent, respectively, as a function of c/c^*, where c and c^* are the solution concentration and the overlap concentration. Inset: D is rescaled by D_{SE}, which is the prediction of the Stokes−Einstein relation with the bulk solution viscosity and the hydrodynamic radius R_H determined by Dynamic Light Scattering. D/D_0 plotted against (b) c/c^* $(M_{w,f}/M_{w,g})^{-1/8}$, (c) R_H/ξ, and (d) $R_H/\xi(M_{w,f}/M_{w,g})^{3/8}$, where ξ is the correlation length in the solution, and $M_{w,f}$ and $M_{w,g}$ are the molecular weights of the free and grafted polymers, respectively. Lines indicate scaling exponent −2 in the scaling theory by Cai et al. [adapted from ref 57].

polymer melts (Figure 16a). They have compared the diffusion coefficients of nonsticky and sticky nanoparticles and found the diffusion coefficients of sticky nanoparticles are smaller within the explored range of melt chain molecular weight M_w (Figure 16b). Their further analysis showed that a long-lived adsorption layer of thickness proportional to $M_w^{1/2}$ enlarges the effective radius of the sticky nanoparticles with respect to the bare particle size and thus slows down the particle diffusion (Figure 16c). A bound polymer layer has also been observed for nanoparticles that interact favorably with an entangled polymer melt. Griffin et al.[30] measured the diffusion of silica nanoparticles in P2VP melts using Rutherford backscattering spectrometry. The diffusion coefficient of the particles with diameter $2R_{NP} \approx 3a$ is well described by the Stokes−Einstein relation, but with the effective particle radius R_{eff} exceeding R_{NP} by an amount comparable to the thickness of a bound polymer layer, which is shown to scale with the melt chain molecular weight as $M_w^{1/2}$.

III. Tethered and adsorbed polymers both target the nanoparticle polymer interface. A related open question concerns the slippage of a polymer matrix over a nanoparticle surface. The slippage of a fluid at a solid surface is quantified by the slip length L_s. Navier determined $L_s = \eta/\zeta$, where η and ζ are the viscosity and friction coefficient of the fluid, respectively. The derivation by Navier was based on the balance of the interfacial friction per unit surface area and the shear stress of the fluid on the surface. Using the same principle of interfacial friction balancing shear stress, de Gennes described theoretically the slippage of a polymer liquid over a nonadsorbing smooth surface.[156] The predicted dependence of L_s on polymer molecular weight has been observed in experiments.[157] The Navier-de Gennes' model for a nonadsorbing surface was later generalized to describe the slippage of a polymer fluid over a surface with permanent chemically grafted polymers.[158,159] Both the conformations and dynamics of the grafted chains alter the fluid−solid interface and thereby the polymer slippage behavior, leading to the dependence of L_s on the grafting density, the degree of entanglements between grafted and bulk polymers, and the rate of the polymer flow. In the context of polymer slippage over a nanoparticle surface, the curvature effect needs to be addressed. For simple fluids, a curvature correction has been introduced based on expressing Navier's model in tensorial form and then applying a coordinate invariant generalization of it to

https://doi.org/10.1021/acs.macromol.3c00260
Macromolecules 2023, 56, 3809−3837

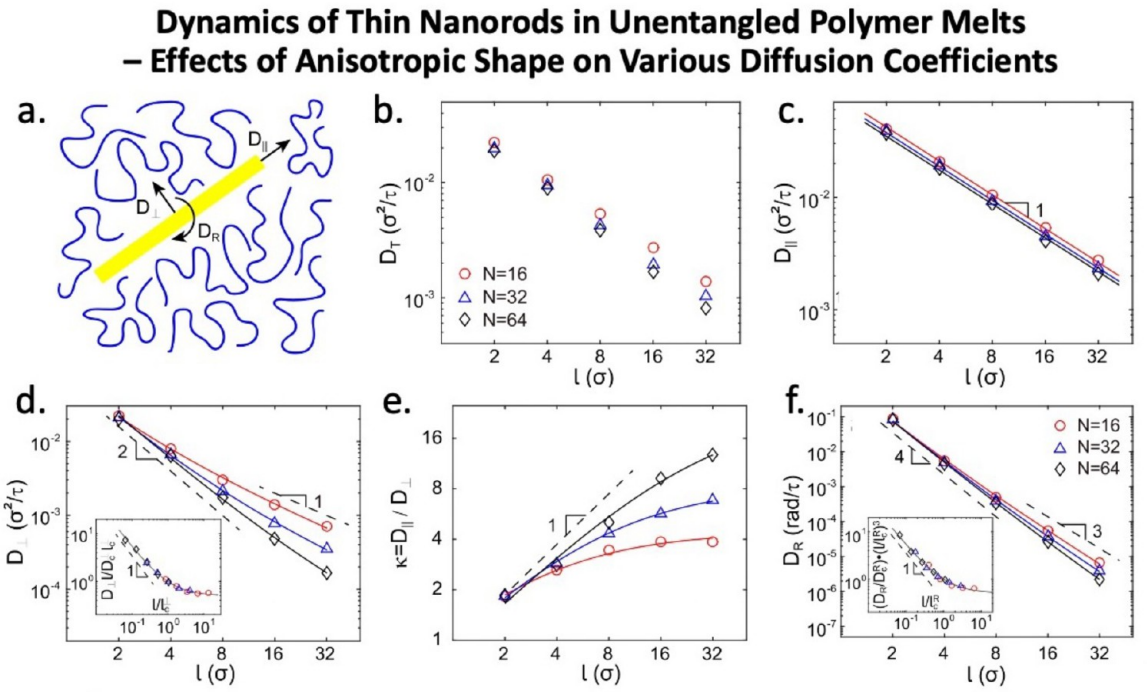

Figure 18. (a) Schematical illustration of a thin nanorod in an unentangled polymer melt. The l-dependence of (b) the overall translational diffusion coefficient D_T, (c) the parallel diffusion coefficient $D_{\parallel}$, (d) the normal diffusion coefficient $D_{\perp}$, (e) the ratio $\kappa = D_{\parallel}/D_{\perp}$, and (f) the rotational diffusion coefficient D_R in molecular simulations [adapted from ref 96].

curved surfaces.[160,161] For the slip of a polymer liquid, systematic studies are needed to revise the slip models of polymers on both nonadsorbing and polymer-grafted surfaces to account for the curvature effect. The role of the interface between tethered polymers and matrix polymers has been demonstrated in the experiments by Poling-Skutvik et al.[57] Using X-ray photon correlation spectroscopy, Poling-Skutvik et al. showed that the diffusion coefficient of PS-grafted silica nanoparticles in PS solution is larger than the prediction of the Stokes−Einstein relation with the hydrodynamic radius R_H determined by the Dynamic Light Scattering (Figure 17a and 17b). They further showed that their experimental data may be collapsed to universal master curves by incorporating the ratio of the free to grafted polymer molecular weights (Figure 17c and 17d), suggesting a soft interaction at the grafted and free polymer interface.

4.3. Dynamics of Thin Nanorods in Polymer Melts—Effects of Anisotropic Particle Shape. Going beyond the spherical shape, nanoparticles with high aspect ratios, particularly nanorods, have been used both as components of functional polymer nanocomposites[162] and in rod-based microrheology experiments on polymers.[45] The highly anisotropic shape of a nanorod enriches features of the diffusion behavior of nanoparticles in a polymer matrix. In addition to the diffusion coefficient D_T for the overall center-of-mass translational diffusion, there are 3 additional diffusion coefficients for the nanorod diffusion, $D_{\parallel}$ and $D_{\perp}$ for the translational diffusion parallel and normal to the rod axis, respectively, as well as D_R for the rotation of the rod. In the continuum limit where both the length l and diameter d of a rod are larger than solvent molecules, the theoretical results for the diffusion coefficients are $D_{\parallel} = k_BT \ln(l/d)/2\pi\eta_s l$, $D_{\perp} = k_BT \ln(l/d)/4\pi\eta_s l$, and $D_R = k_BT[\ln(l/d) - \gamma]/\pi\eta_s l^3$), where η_s is the solvent viscosity, and γ is a numerical correction.[9] The logarithmic terms reflect the speed-up in mobility due to the hydrodynamic coupling between distant portions of a nanorod. As in the diffusion of spherical nanoparticles, when the dimensions of a nanorod become comparable or smaller than the structural length scales in the polymer matrix, such as polymer chain size R in an unentangled polymer melt and entanglement mesh size a in an entangled polymer melt, the continuum theory is anticipated to break down.

A simple model system has been studied in molecular simulations to reveal the effects of anisotropic shape on the diffusion of nanoparticles.[96] In the simulations, the rod diameter is comparable to the polymer bead size σ, while a rod of length l is composed of l/σ beads along a straight line. This simple model of monomerically thin nanorods indeed demonstrates the breakdown of the continuum theory.

(1) The diffusion parallel to the rod axis corresponds to the easy direction of nanorod motion. Simulations show that for sufficiently long melt chains, the parallel diffusion coefficient $D_{\parallel}$ decreases linearly with increasing l in an unentangled polymer melt (Figure 18c). The linear relation arises from screening the hydrodynamic coupling between different portions of the rod. With no hydrodynamic coupling, the friction coefficient of the rod is the sum of the individual monomeric friction coefficients, $\zeta_{\parallel} \approx \zeta_0 (l/\sigma)$.

(2) The diffusion normal to the rod axis corresponds to the hard direction of nanorod motion. The decrease of $D_{\perp}$ with increasing l exhibits a crossover from $D_{\perp} \sim l^{-2}$ to $D_{\perp} \sim l^{-1}$, as shown in Figure 18d. This l-dependence results from the progressive coupling of the rod to the melt, which gives rise to a crossover from $\zeta_{\perp} \sim l^2$ to $\zeta_{\perp} \sim l$. The effective viscosity $\eta_{\perp,\text{eff}}$ for the normal diffusion is only a fraction of the bulk melt viscosity η_{melt} if the rod is not sufficiently long with respect to the bulk melt chain size R. The simulation results suggest that the effective viscosity

https://doi.org/10.1021/acs.macromol.3c00260
Macromolecules 2023, 56, 3809−3837

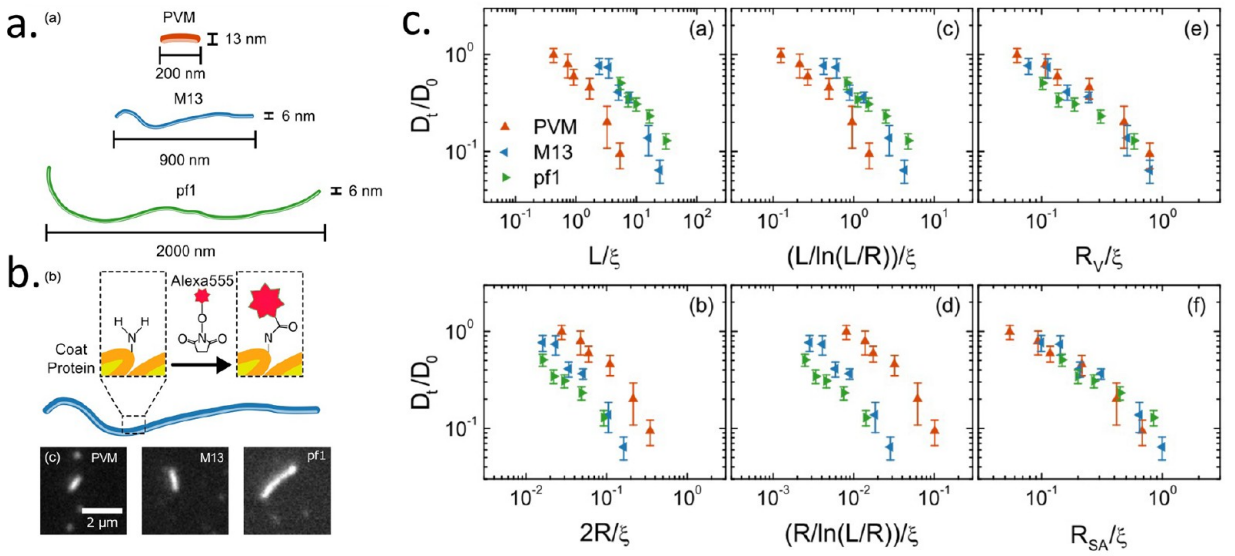

Figure 19. (a). Schematic illustration of PVM, M13, and pf1 viruses. (b) Fluorescence micrographs of the virus nanoparticles labeled with Alexa555. (c) D_t/D_0, where D_t and D_0 are the translational diffusion coefficients of fluorescently labeled virus nanoparticles in the solutions of partially hydrolyzed polyacrylamide (HPAM) and in the pure solvent 1X PBS, respectively, as functions of various normalized length scales. L and R are the length and radius of the virus particle, respectively. ξ is the correlation length of the polymer solution. $R_V = (3R^2L/4)^{1/3}$ and $R_{SA} = (RL/2)^{1/2}$ [adapted from ref 73].

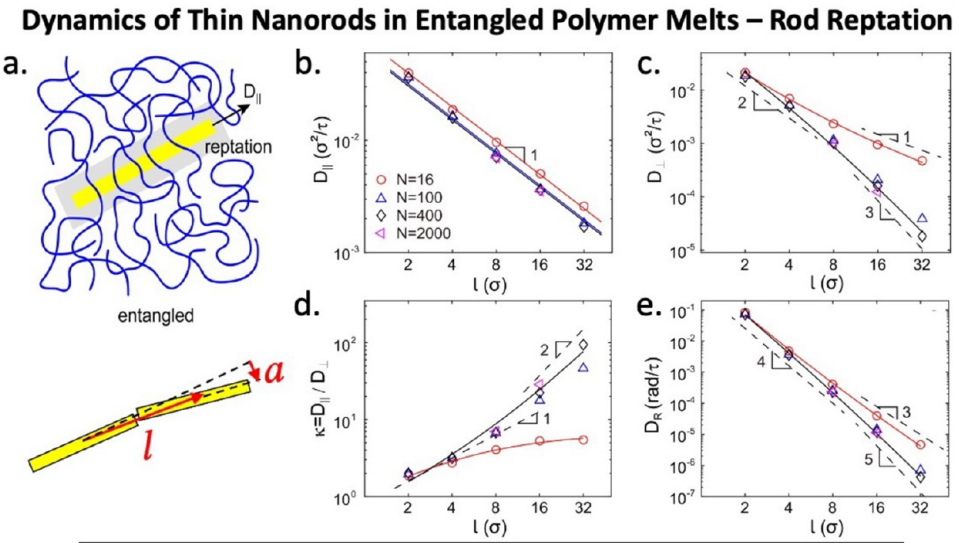

Figure 20. (a) Schematical illustration of the reptation of a thin nanorod in an entangled polymer melt. The l-dependence of (b) the parallel diffusion coefficient $D_{\parallel}$, (c) the normal diffusion coefficient $D_{\perp}$, (d) the ratio $\kappa = D_{\parallel}/D_{\perp}$, and (e) the rotational diffusion coefficient D_R in molecular simulations [adapted from ref 96].

$\eta_{\perp,\mathrm{eff}} \sim l$ before leveling off such that $\zeta_{\perp} \approx \eta_{\perp,\mathrm{eff}}\, l \sim l^2$. $\eta_{\perp,\mathrm{eff}}$ is eventually constant and $\zeta_{\perp} \approx \eta_{\perp,\mathrm{eff}}\, l \sim l$ if the rod is sufficiently long with respect to R. Note that the scaling $D_{\perp} \sim l^{-1}$ is identical to the l-dependence of the diffusion coefficient in the continuum theory[9] but with the logarithmic term for the hydrodynamic interactions excluded.

(3) The ratio $\kappa = D_{\parallel}/D_{\perp}$ increases linearly with l before leveling off, as shown in Figure 18e. The anisotropy between the diffusion coefficients in the parallel and normal directions originates from the different values of effective viscosity for the two directions and is a feature distinctively different from the isotropic diffusion of spherical nanoparticles.

The mean squared angular displacement (MSAD) of a nanorod is $\langle|\vec{u}(t) - \vec{u}(0)|^2\rangle$, where $\vec{u}(t)$ is the time-dependent unit vector along the rod axis. The rotational diffusion coefficient D_R of the nanorods in the simulation is extracted from the long-time limit of MSAD, which is $2[1-\exp(-2D_R t)]$. The rotational diffusion time $\tau_R = 1/(2D_R)$ is essentially the time scale for the decorrelation of the nanorod orientation. The l-dependence of D_R exhibits a crossover from $D_R \sim l^{-4}$ to $D_R \sim l^{-3}$, as shown in Figure 18f. This is consistent with the relation $D_R \sim D_{\perp} l^{-2}$, as in the continuum theories.[9] The microscopic origin of the relation is that the same effective viscosity determines the translational diffusion in the normal direction and the rotational diffusion. The rotational diffusion affects the transformation of $D_{\parallel}$ and $D_{\perp}$ in the body frame of the rod to the overall translational diffusion coefficient D_T in the lab frame. The

https://doi.org/10.1021/acs.macromol.3c00260
Macromolecules 2023, 56, 3809−3837

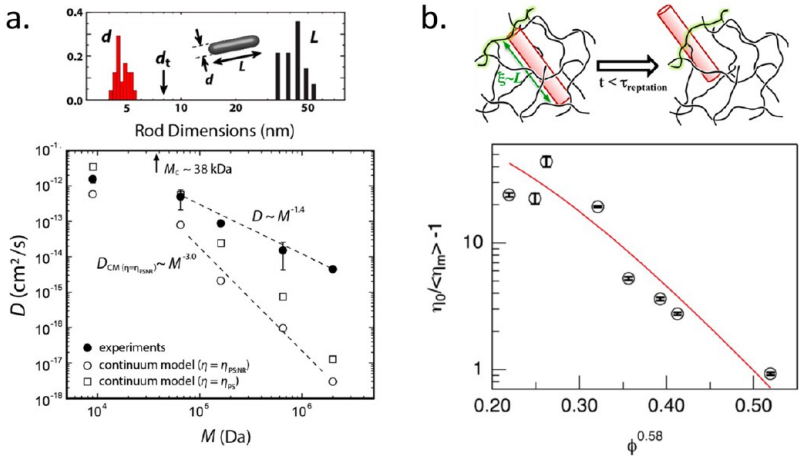

Figure 21. (a) Diffusion coefficient D of TiO_2 nanorods in a polystyrene (PS) melt. The rod diameter d and the rod length L are smaller and larger than the tube diameter d_T of the PS melt, respectively. Solid symbols and open symbols are experiment data from the Rutherford back scattering and the theoretical predictions of the continuum model, respectively [adapted from ref 167]. (b) X-ray photon correlation spectroscopy (XPCS) and rheology studies of the translational dynamics of gold nanorods in the semidilute solutions of entangled wormlike micelles. Entanglement mesh size decreases from larger than the rod length L to approximately equal to the rod diameter d, as the micelle volume fraction ϕ increases. Symbols show $\eta_0/\langle\eta_m\rangle - 1$, where η_0 and $\langle\eta_m\rangle$ are the macroscopic viscosity and the viscosity obtained from the nanorod diffusivity in the micelle solution, versus $\phi^{0.58}$. The red line shows the fit of the experiment data to the hopping diffusion model by Cai et al. [adapted from ref 39].

equation $\tilde{D}_T = (D_\parallel + 2D_\perp)/3$, which assumes the parallel diffusion mode and two normal diffusion modes are independent in the lab frame, is valid if the rotational diffusion is sufficiently slow such that the rotational diffusion lags the translational diffusion. Otherwise, $\tilde{D}_T$ overestimates the translational diffusion coefficient, as the rotational diffusion couples the parallel and normal diffusion coefficients in the body frame. This coupling of translational and rotational diffusions was observed in the simulations.[96]

The simulation results from decomposing the overall translational diffusion to the diffusion parallel and normal to the rod axis motivated a scaling ansatz that the effective viscosity η_{eff} for the overall diffusion coefficient D_T is a geometric mean of the monomeric viscosity η_0 and the maximum viscosity η_{max}, which corresponds to the viscosity for the parallel and normal diffusion, respectively. Similar to $\eta_{eff} \approx \eta_0\ (d^2/b^2)$ for the spherical nanoparticles in an unentangled linear polymer melt, $\eta_{max} \sim l^2$ for l smaller than the polymer chain size R. This geometric-mean conjecture reflects the effect of anisotropic shape and was proposed first by Aponte-Rivera and Rubinstein to describe the rheology of oppositely charged polyelectrolytes.[163]

One experimental realization of thin nanorods in polymers was based on filamentous viral nanoparticles. Smith et al.[73] used fluorescence microscopy to examine the translational dynamics of three different flexible filamentous vial nanoparticles in the semidilute solutions of partially hydrolyzed polyacrylamide (Figure 19a and 19b). They observed that the translational diffusion coefficients for different viral nanoparticles at different solution concentrations do not collapse onto the universal curve predicted by the continuum theory for rodlike nanoparticles. Instead, an apparent collapse of the diffusivity data was observed when plotted against the ratio of the solution correlation length ξ and a length scale intermediate between the virus radius R and length L. Specifically, two length scales $R_V = (3R^2L/4)^{1/3}$ and $R_{SA} = (RL/2)^{1/2}$, which correspond to the radius of a sphere with the same volume and the same surface area as the filamentous particle, respectively, were used. The results by Smith et al. demonstrated the effects of anisotropic particle shape on the nanoparticle−polymer coupling, which cause a breakdown of the continuum theory.

Simulations for thin nanorods in entangled polymer melts have also been performed.[96] The parallel diffusion coefficient $D_\parallel$ decreases with increasing l in entangled polymers (Figure 20b), also because of the screening of hydrodynamic interactions. The normal diffusion coefficient exhibits a crossover from $D_\perp \sim l^{-2}$ to $D_\perp \sim l^{-3}$ (Figure 20c), different from the counterpart in unentangled polymer melts. The anisotropy ratio increases first as $\kappa \sim l$ and then as $\kappa \sim l^2$ (Figure 20d), indicating the highly anisotropic motion of the long nanorods in entangled polymers. The l-dependence of the rotational diffusion coefficient also exhibits a different behavior going from $D_R \sim l^{-4}$ to $D_R \sim l^{-5}$ (Figure 20e), but it still agrees with $D_R \sim D_\perp\ l^{-2}$. These simulation results demonstrate the effects of the constraints on nanorod motion due to the entanglement network. They agree with de Gennes' rod reptation model.[164] As shown in Figure 20a, as the rod reptates over a distance of its length l with diffusivity $D_T \approx D_\parallel$, the displacement due to normal diffusion $\approx a$. From $l^2/D_\parallel \approx a^2/D_\perp$, one obtains $D_\perp \approx D_\parallel\ a^2/\ l^2 \sim l^{-3}$ for slender nanorods in entangled chains.

The anisotropic motion of a stiff filament reptating in a polymer matrix with topological constraints has been studied by Fakhri et al.[165] Using near-infrared video microscopy, they followed the reptating path of individual single-walled carbon nanotubes (SWNTs) in agarose gels. The trajectory of the SWNT is highly anisotropic with the diffusion parallel to the reptating path dominating over the diffusion normal to the path, and the diffusion is isotropic finally at time scales longer than the rotational diffusion time. Fakhri et al.also found that even small bending flexibility of the SWNT enhances the diffusion, and the rotational diffusion follows the prediction of Odijk's theory[166] for semiflexible rods rather than Doi's theory for rigid rods.[9]

Experiments of nanorods in an entangled polymer matrix have been performed by Choi et al.[167] They used Rutherford backscattering spectrometry to measure the concentration profiles of titanium dioxide (TiO_2) nanorods in polystyrene (PS) melts with varying molecular weights M. The diffusion coefficient D of the nanorods decreases as $M^{-1.4}$, which is a

https://doi.org/10.1021/acs.macromol.3c00260
Macromolecules 2023, 56, 3809−3837

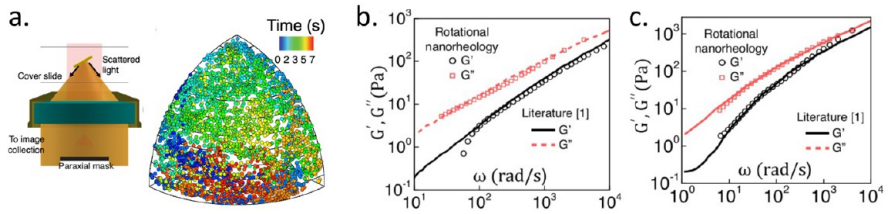

Figure 22. (a) Time-dependent gold nanorod orientation mapped into a single octant. Data from the scattering of the gold nanorod in a poly(ethylene oxide) (PEO) solution under a dark-field microscope. (b) and (c) are storage and loss moduli for the PEO solutions with 6.7% w/w and 12.2% w/w, respectively. Results from the nanorod-based rotational rheology (symbols) are compared with the microrheology data in the literature (lines) [adapted from ref 45].

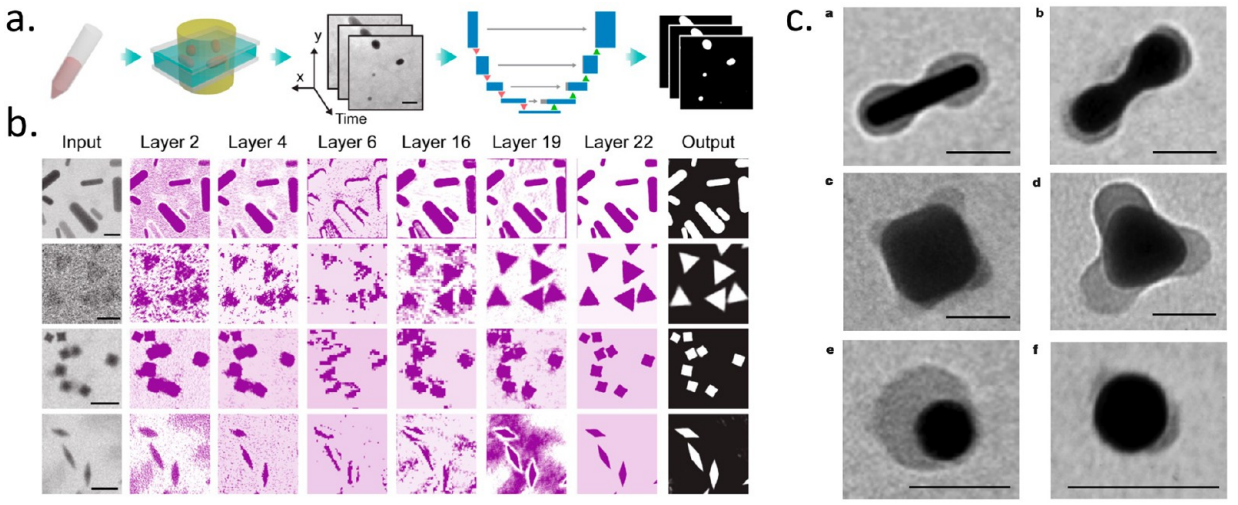

Figure 23. (a) Image segmentation for the liquid-phase transmission electron microscopy (TEM) based on U-Net convolutional neural network, a machine learning algorithm. (b) Representative data flow in the U-Net models for the imaging of nanorods, triangular nanoprisms, concave nanocubes, and bipyramids [adapted from ref 170]. (c) TEM images of noble metal nanoparticles (dark cores) of various shapes with additional polymer patches (light shells) [adapted from ref 171].

weaker dependence compared to the prediction M^{-3} using the continuum theory (Figure 21a). Since the nanorod length L is larger than the entanglement mesh size d_T of the PS melt but the nanorod thickness d is smaller than d_T, Choi et al. attributed the enhanced diffusivity to the anisotropic nanorod shape that results in the decoupling of the nanorod from the bulk viscosity. This argument agrees with the picture of rod reptation. Lee et al.[39] studied the mobility of Au nanorods within entangled wormlike micelle solutions using X-ray photon correlation spectroscopy (XPCS). An effective viscosity $\langle \eta_m \rangle$ was computed from the terminal diffusion coefficient. $\langle \eta_m \rangle$ is smaller than the bulk viscosity η_0 at low micelle volume fraction ϕ, but it increases toward η_0 as ϕ increases and entanglements set in. The ϕ-dependence of $\eta_0/\langle \eta_m \rangle - 1$ is well fit to the hopping diffusion model developed by Cai et al.[88] (Figure 21b).

Open Questions. I. Increasing the nanorod thickness to be above the Kuhn monomer size may be one extension of the theoretical and computational research on the dynamics of nanorods in polymer melts. This extension is meaningful in terms of making a closer connection to experiments where thick nanorods are often used. One would expect as the thickness increases the effective viscosity for the diffusion in the easy direction parallel to the rod axis increases with respect to the monomeric viscosity and exhibits a dependence on the rod thickness. This change would affect both the anisotropy in the overall translational diffusion and the rotational diffusion. For sufficiently thick nanorods, the continuum theory for rod diffusion is anticipated to be applicable. In the experiments by Molaei et al.,[45] the nanoscale rheology probed by following the rotation of gold nanorods in a polymer solution agrees with the microrheology probed using spherical colloidal particles, as shown in Figure 22. The generalized Stokes−Einstein relation was extended to covert MSAD of the probe nanorod to the stress relaxation modulus $G(t)$. Other than the rod thickness, the diffusion of a nanorod is anticipated to depend on the surface roughness of the nanorod. Molecular simulations have demonstrated the effects of surface roughness on the phase behavior of thin nanorods in polymers[168] and may reveal the effects of surface roughness on the dynamics of thin nanorods as well. Further extension of the research on nanorods in polymer melts may include the flexibility of the nanorod. This extension is relevant to the experiments that use carbon nanotubes[165] and filamentous viral nanoparticles[73] with intrinsic flexibility to explore the nanorod-polymer coupling. The dynamics of rigid nanorods are anticipated to be modified by the elastic bending modes of the rod itself. Adding the studies of rod thickness, surface roughness, and rod flexibility will broaden the fundamental understanding of nanorod-polymer coupling. For future experiments, recent advances in the design principles of colloidal nanorod heterostructures[169] may be utilized for the precise control of nanorod geometry as well as the tracking of nanorods based on the optical properties of semiconductor nanocyrstals.

II. Nanoparticles with other nonspherical geometries may be studied to further understand the role of anisotropic shapes in nanoparticle−polymer coupling. As shown in Figures 23a and

https://doi.org/10.1021/acs.macromol.3c00260
Macromolecules 2023, 56, 3809−3837

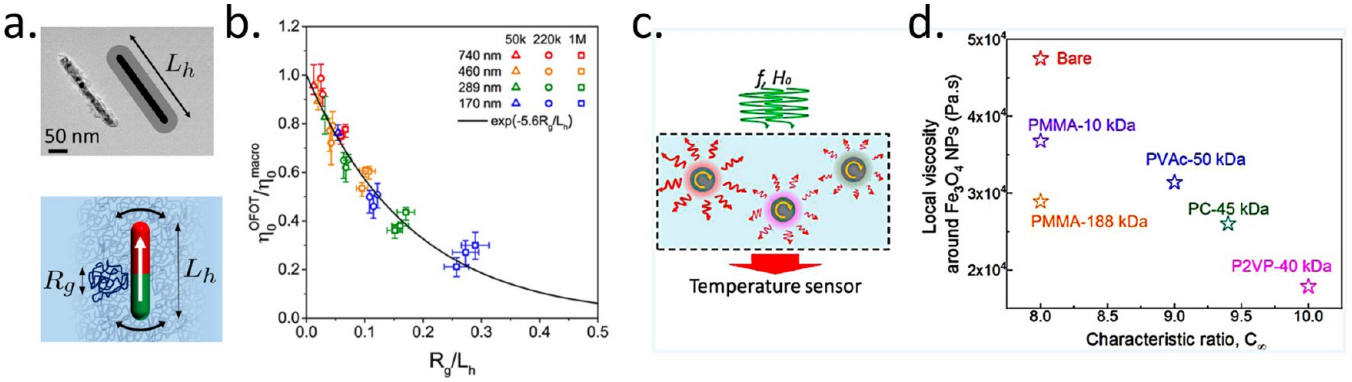

Figure 24. (a) TEM image of a Ni nanorod with a rough surface due to irregular oxide (upper panel) and schematic illustration of a Ni nanorod in a solution of polymers with the radius of gyration R_g for the oscillating-field optical transmission (OFOT) measurements of the apparent viscosity η_0^{OFOT}. L_h is the hydrodynamic length of the nanorod. (b) $\eta_0^{OFOT}/\eta_0^{macro}$ vs R_g/L_h from the OFOT measurements of the Ni nanorods with indicated L_h in the solutions of poly(ethylene oxide) (PEO) with indicated molecular weights. η_0^{macro} is the zero rate viscosity of the solution. The solid line is the best fit to an exponential function [adapted from ref 58] (c) Schematic illustration of the magnetic heating experiments based on the rotation of magnetic nanoparticles in a polymer matrix. (d) Local viscosity around the nanoparticles in a PMA melt. Results were obtained from the magnetic heating experiments using the bare Fe_3O_4 nanoparticles and Fe_3O_4 nanoparticles with adsorption layers of indicated polymers and molecular weights [adapted from ref 70].

22b, nanoparticles of various shapes, such as nanorods, triangular nanoprisms, convave nanocubes, and bipyramids, can be synthesized, and their dynamics and self-assembly behavior can be visualized using the liquid-phase transmission electron microscopy with the aid of a machine learning algorithm for image analysis.[170] Furthermore, the shape of inorganic nanoparticles may be fine-tuned by the surface patterning with polymer patches, as demonstrated by Choueiri et al.[171] One particular system for future study may be nanoplates in polymer melts. Krook et al.[172] have combined experiments and simulations to probe the aligned assemblies of nanoplates within ordered block copolymer lamellae. The small and monodisperse nanoplates in the self-assembly experiments may be used in future experiments on nanoplate dynamics within a polymer matrix. Unlike nanorods, nanoplates possess two easy directions for diffusion: the two orthogonal directions within the plane of a nanoplate, and one hard direction for diffusion, which is the direction normal to the nanoplate plane. In unentangled polymer melts, future research may examine the decomposition of the overall translational diffusion to the three orthogonal components in the body frame as well as the rotational diffusion of the nanoplates. In entangled polymer melts, a thin plate with a side length larger than the entanglement mesh size a would be trapped but may be able to diffuse via a hopping diffusion mechanism if the side length is slightly above a. In general, the hopping diffusion model[88] may be extended from spherical nanoparticles to those with various nonspherical geometries.

III. In contrast to the clear visibility of the rotation of a nanorod, the rotation of a spherical nanoparticle is obscured by the more recognizable translational motion. As a result, the rotational diffusion of spherical nanoparticles in polymer melts has been less explored. Similar to the Stokes−Einstein relation for the translational diffusion of a spherical particle in a viscous continuum, there is Stokes−Einstein-Debye relation $D_r = k_BT/\pi\eta d^3$ for the rotational diffusion of the particle in a viscous continuum. The breakdown of the Stokes−Einstein-Debye relation is anticipated for a nanoparticle with sizes smaller or comparable to the structural length scales of a polymer melt. Future theoretical and computational research may be designed to specifically explore this breakdown and further clarify the length-scale and time-scale dependent coupling between nanoparticle rotation and surrounding polymers. On the experiment side, the rotation of a magnetic nanoparticle under a magnetic field has been recently used to measure the local viscosity surrounding the nanoparticles. Gratz and Tschöpe[58] studied the rotational motion of Ni nanorods in poly(ethylene oxide) solutions by oscillating magnetic field-dependent optical transmission (OFOT) measurements (Figure 24a). The local viscosity η_0^{OFOT} extracted from the nanorod rotation exhibits a size-dependent deviation from the bulk viscosity η_0^{macro} determined by the macroscopic rheology experiment (Figure 24b). The reduction of entanglements with decreasing polymer solution concentration was attributed as the origin of the observed size effect on $\eta_0^{OFOT}/\eta_0^{macro}$. Wu et al.[70] measured the local viscosity of interfacial layers in polymer nanocomposites based on magnetic heating due to the rotation of a nanoparticle under a high-frequency alternating magnetic field (Figure 24c). The experiments revealed a dependence of the local viscosity on the rigidity of polymers in the interfacial layer (Figure 24d). Opportunities are present in the research on rotational diffusion of nanoparticles in a polymer matrix. For the state-of-the-art experimental techniques of tracking the rotational diffusion of anisotropic nanoparticles, readers are advised to read the review by Rose et al.[62]

4.4. Active Dynamics of Force-Driven Thin Nanorods in Polymer Melts—Non-Equilibrium Effects. Activeness may be introduced to the motion of nanoparticles in a polymer matrix by applying an external field such as a magnetic field,[173,174] an electric field,[175] near-infrared light[176] and ultra sound[177,178] or by a chemistry-based mechanism of self-propulsion.[179−184] Activeness allows the motion of nanoparticles to overcome the passive dynamics that are coupled with the viscoelasticity of the polymer matrix. Instead of the randomness of the passive dynamics, activeness results in definite and directed motion, which is essential for the control of nanoparticles in functional nanocomposites and the manipulation of particle-based nanomotors in bioimaging and drug delivery.

A combination of molecular simulations and scaling theory has been used to study the effects of activeness on the interplay of thin nanorods and an unentangled polymer melt. In the

https://doi.org/10.1021/acs.macromol.3c00260
Macromolecules 2023, 56, 3809−3837

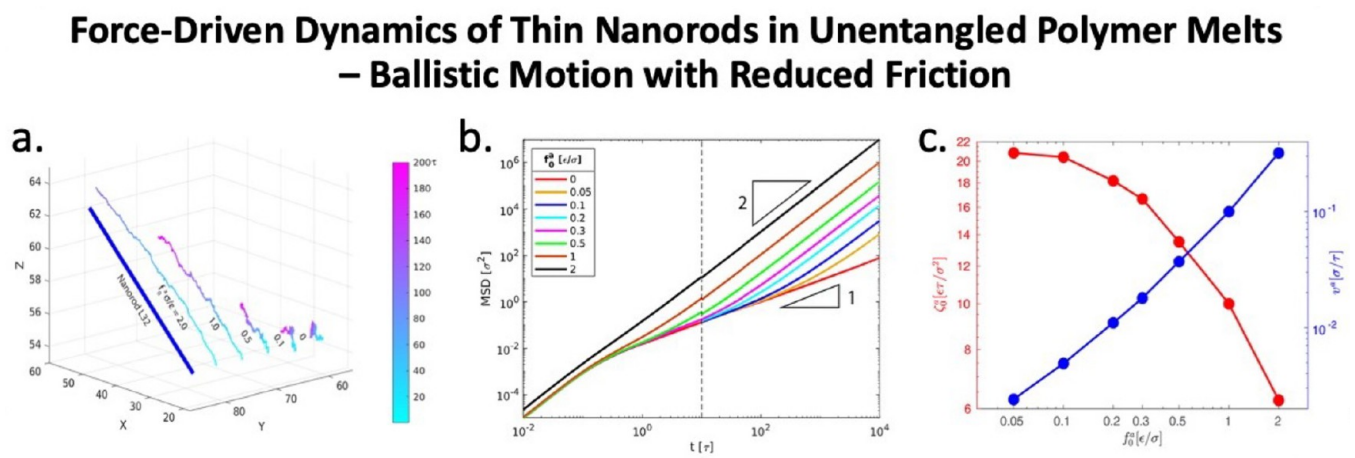

Figure 25. (a) Molecular dynamics trajectories and (b) MSDs of force-driven thin nanorods in unentangled polymer melts at indicated active force per monomer length scale f_0^a. (c) The speed of force-driven ballistic motion v^a and the friction coefficient per monomer ξ_0^a as functions of f_0^a [adapted from ref 97].

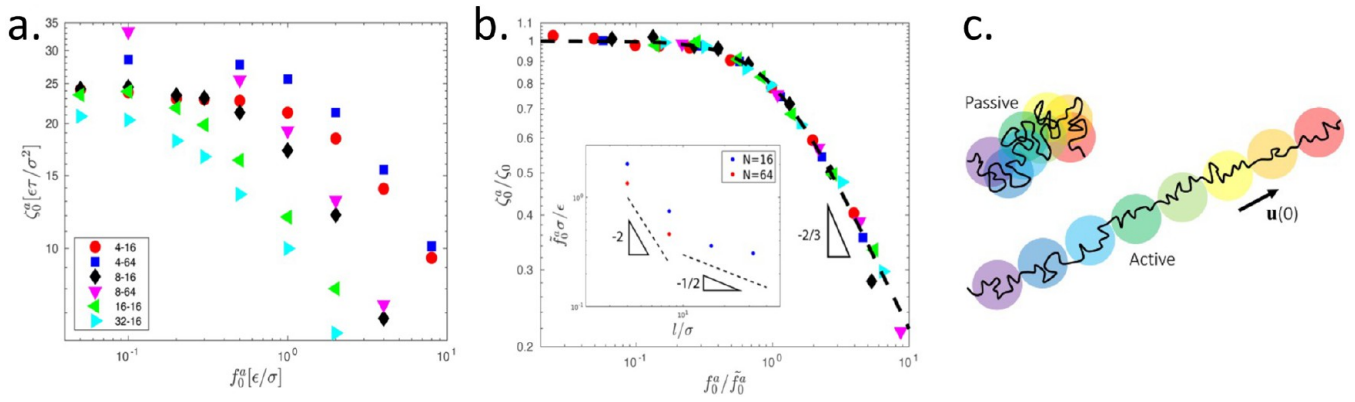

Figure 26. (a) The friction coefficient per monomer ζ_0^a as a function of the active force per monomer f_0^a in the molecular simulations with indicated $l-N$, where l and N are the thin rod length and melt chain length, respectively. (b) A master curve is constructed by rescaling ζ_0^a and f_0^a with ζ_0 and $\tilde{f}_0^a$, respectively. Power-law exponents from the scaling theory are indicated. Inset: The threshold $\tilde{f}_0^a$ for friction reduction as a function of l. Dashed lines indicate the power laws in the scaling theory. (c) Schematic illustration of the active blobs in the time domain. Colors of increasing wavelength indicate the temporal sequence of the blobs [adapted from ref 97].

simulations, nanorods are monomerically thin and made of connected LJ beads as a rigid body, and unentangled polymer chains are modeled using the bead−spring model. Activeness is introduced by applying a constant force uniformly along the initial rod axis, which facilitates the arrival of the steady state in the simulations. The strength of activeness is quantified by the active force per monomer length scale f_0^a. The trajectory of a thin rod over the same time is transformed from a random-walk coil to a more directed conformation with increasing f_0^a, as illustrated in Figure 25a. The motion of a thin rod is quantified by the MSD $\langle \Delta r^2(t) \rangle$. Compared with the passive motion ($f_0^a = 0$) that reaches a diffusive regime at long time scales, the active motion ($f_0^a > 0$) is characterized by the ballistic motion with $\langle \Delta r^2(t) \rangle \sim t^2$ at long time scales, as shown in Figure 25b. Furthermore, the ballistic motion starts at shorter time scales with increasing f_0^a. The ballistic speed v^a defined as $\sqrt{\langle \Delta r^2(t) \rangle / t^2}$ in the terminal ballistic regime increases with f_0^a (blue symbols in Figure 25c). However, the friction coefficient per monomer, $\zeta_0^a = f_0^a/v^a$, decreases as f_0^a increases (red symbols in Figure 25c), indicating that the activeness makes it easier for the nanorod to pierce through the polymer matrix. Additional analysis shows that the force-driven ballistic motion suppresses the rotational diffusion of the rod and cuts off the decorrelation of the rod axis with time.

A scaling theory was developed to understand the simulation results for the active motion of force-driven nanorods in a polymer melt. The time scale at which the motion becomes ballistic is determined by equating the MSD for a nanorod in the active ballistic motion $(v^a t)^2 \approx (f_0^a/\zeta_0^a)^2 t^2$ and the MSD for a thin nanorod in thermal diffusion $\langle \Delta r^2(t) \rangle \approx [k_B T/\zeta_0^a(l/\sigma)]t$, where the friction coefficient is $\zeta_0^a(l/\sigma)$ for the rod consisting of l/σ monomers. The time scale $\tau_{\text{ballistic}}$ at which the two MSDs are comparable separates the ballistic motion for $t > \tau_{\text{ballistic}}$ from the passive motion for $t < \tau_{\text{ballistic}}$. With increasing f_0^a, $\tau_{\text{ballistic}}$ becomes smaller than the terminal diffusion time τ_{relax} of the melt chains, meaning the active force renews the local environment of the nanorod at a rate that only allows the completion of local chain segments rather than the entire melt chains. Using the Rouse

https://doi.org/10.1021/acs.macromol.3c00260
Macromolecules 2023, 56, 3809−3837

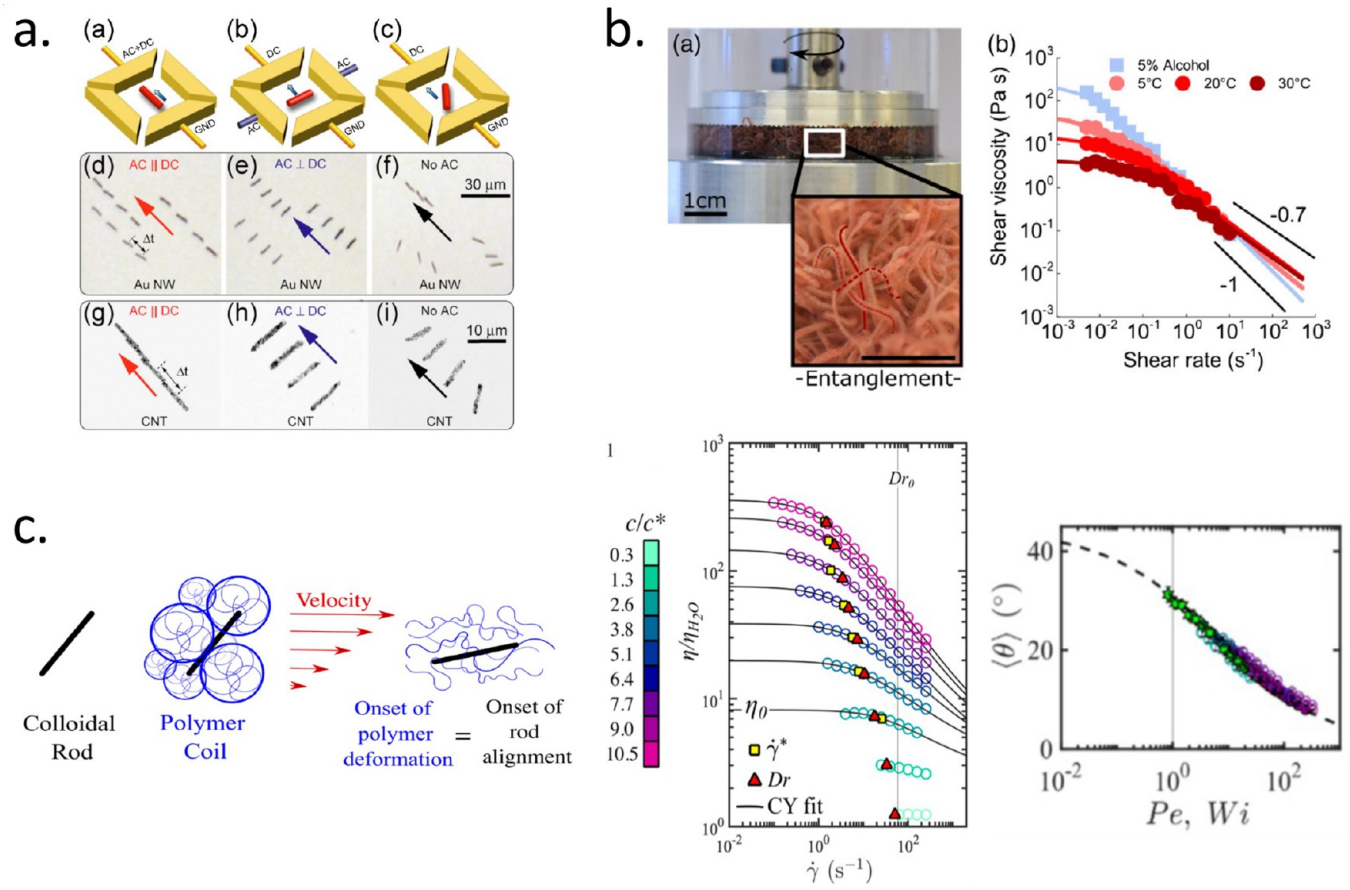

Figure 27. (a) Precise control of the ballistic motion and orientation of Au nanowires and multiwalled Carbon Nanotubes (CNTs) in water by using the combination of dc and ac electric fields [adapted from ref 175]. (b) Rheology of entangled active polymer-like *T. tubifex* worms exhibits reduced zero rate viscosity and weaker shear thinning with increasing activity. Worm activity increases as alcohol is removed and temperature is increased [adapted from ref 185]. (c) The alignment of the rods made of cellulose nanocrystals during the shear thinning of poly(ethylene oxide) (PEO) solutions depends on the Weissenberg number W_i [adapted from ref 79].

model, the number of monomers g^a in a relaxed chain segment is derived from $\tau_g^a \approx \tau_0 (g^a)^2 \approx \tau_{\text{ballistic}}$. The result shows g^a decreases as $(f_0^a)^{-4/3}$. The friction coefficient $\zeta^a \approx \eta_{\text{eff}}{}^a l \sim (f_0^a)^{-2/3}$. The effective viscosity η_{eff}^a is the geometric mean of η_0 and the viscosity $\eta_{\max} \approx \eta_0 g^a \sim (f_0^a)^{-4/3}$ of the local chain segments, which is a consequence of the anisotropic nanoparticle shape, as discussed in Section 4.3. Simulation results of ζ_0^a vs f_0^a for different combinations of rod length l and melt chain length N are collapsed to a master curve that supports the scaling relation for the power-law reduction of ζ^a above a threshold $\tilde{f}_0^a$, as shown in Figure 26a and 26b. The threshold $\tilde{f}_0^a$ decreases with increasing l and exhibits different l-dependencies for l smaller and larger than the polymer size R (see inset to Figure 26b).

Additional scaling analysis showed that by the time scale $\tau_{\text{ballistic}} \approx \tau_g^a$, the work performed by the applied active force $w^a \approx f^a v^a \tau_{\text{ballistic}}$ is comparable to the thermal energy $k_B T$. Recall that the thermal diffusion arises from thermal energy $k_B T$, as shown in the Einstein relation $D = k_B T/\zeta$. The condition $w^a > k_B T$ is the reason why the long-time ballistic motion of the nanorod is not affected by the thermal fluctuation. The center-of-mass trajectory in the time domain for the force-driven active nanorod may be described as a stretched array of "active blobs", as illustrated in Figure 26c. The stretched conformation replaces the random-walk coil conformation of the trajectory for the passive dynamics of the nanorod. Each blob corresponds to a time scale $\tau_{\text{ballistic}} \approx \tau_g^a$ and a length scale comparable to the ballistic MSD $(v^a \tau_{\text{ballistic}}^a)^2$. The effects of active force on the trajectory in the time domain are analogous to the effects of a pulling force on the conformation of a single polymer chain in real space, which are described by the famous tension blobs in polymer scaling theory.[128]

Open Questions. I. The research on force-driven thin nanorods in unentangled polymer melts may be extended to explore whether the force-driven ballistic motion occurs for spherical nanoparticles, for which there are no preferential directions for easier diffusion, as well as for nanorods in entangled polymers where topological constraints on the nanorods present a barrier for the force-driven motion. If force-driven ballistic motion could take place, then one may further study the length- and time-scale dependent features of the coupling between force-driven nanoparticles and surrounding polymers. Even if the external force is not sufficiently large to take over and make the nanoparticle motion ballistic, the force may still affect the thermal diffusion of the nanoparticles. One example is active microrheology[186−189] in which a colloidal particle experiences a driving force and explores the viscoelasticity of a medium in a force-driven manner. The viscoelasticity explored may be in the linear response regime or nonlinear regime depending on the strength of the driving force. It is anticipated that studying the length- and time-scale dependent features of the force-driven nanoparticle motion in

https://doi.org/10.1021/acs.macromol.3c00260
Macromolecules 2023, 56, 3809−3837

a polymer melt would aid in the extension of passive nanorheology[102] to active nanorheology.

II. The behavior of active matter generally depends on the rules of imposing activeness. The constant force in the simulations discussed in Figures 25 and 26 may be realized using charged nanorods in electric fields. Fan et al.[175] have demonstrated the precision transport of Au nanowires and multiwalled carbon nanotubes (MWNCTs) using a combination of dielectrophoretic force and electrophoretic force, which control the orientation and the ballistic translation of the nano-objects, respectively (Figure 27a). Other than being externally driven by a force, self-propulsion is a common mechanism of activeness. For example, living worms with natural activeness were used in rheology to study the effects of activeness on entangled polymers by Deblais et al.[185] The experiments showed that with an increasing level of activeness, the zero-rate shear viscosity decreases, while the shear thinning behavior becomes weaker (Figure 27b). It was argued that the bead−spring polymer model with a tangential self-driving force is suitable to describe the polymer-like worms. Self-propelled thin nanorods are good models of active filaments in biological systems. Recent computational and theoretical work by Mandal et al.[190] has demonstrated that a concentrated system of self-propelled active filaments exhibits crowding-enhanced diffusion. In the context of nanoparticle−polymer coupling, one would expect that a self-propelled nanorod possesses a higher flexibility in exploring an entangled polymer melt with topological constraints, compared to a nanorod with a driving force in a fixed direction.

III. The reduction in effective viscosity due to a fast renewal of the local polymeric environment, that is, the force-driven ballistic motion starts at a time scale $\tau_{\text{ballistic}}$ shorter than the terminal relaxation time of the polymer τ_{relax}, can also be achieved for nanoparticle−polymer composites under out-of-equilibrium flow conditions. Polymers under a shear flow with a large Weissenberg number W_i, which is the product of the shear rate $\dot{\gamma}$ and τ_{relax} of the polymers, exhibit shear thinning, which refers to the decrease of the bulk viscosity with increasing $\dot{\gamma}$ (Figure 27c). A nanoparticle embedded in such a strong shear flow is anticipated to experience a reduced local viscosity depending on the particle size with respect to the length scale where polymer chain dynamics is perturbed by the external flow. For nanorods, Calabrese et al.[79] have demonstrated the alignment of cellulose nanocrystalline rods under the shear flow of polymers at large W_i Figure 27d. The onset of polymer shear thinning (reduction in the shear viscosity η) coincides with the onset of the alignment of the rod (reduction in the average angle $\langle\theta\rangle$ with the shear direction). Investigating the nanoparticle−polymer coupling under out-of-equilibrium flow conditions will help design particle-based experiments to investigate nonlinear polymer rheology[191,192] as well as control the processing of nanoparticle−polymer composites under strong nonequilibrium flows such as encountered in 3D additive manufacturing.

5. CONCLUDING REMARKS

The research on the dynamics of nanoparticles in a polymer matrix may be extended to cover more types of polymer matrices.

I. Cross-linking polymer melt chains yields a rubbery network. The hopping diffusion of nanoparticles larger than the cross-linked network mesh size was described in the scaling theory by Cai, Paniukov, Rubinstein,[88] as well as in the microscopic theory by Dell and Schweizer.[89] The Cai-Paniukov-Rubinstein theory focused exclusively on the hopping of nonsticky hard nanoparticles. The Dell-Schweizer theory additionally included the hopping of soft nanoparticles and touched the role of nanoparticle−polymer attraction. For the hopping of nonsticky hard nanoparticles in solvent-free dry polymer networks, the two theories are qualitative different.

(1) The Cai-Paniukov-Rubinstein theory predicted that the step size in the hopping diffusion is on the order of Kuhn monomer size and thus independent of the particle size. The Dell-Schweizer theory predicted that the jump distance in the particle hopping process grows as the confinement (quantified as the ratio of particle size and network mesh size) increases and exhibits a dependence on the particle size.

(2) The Cai-Paniukov-Rubinstein theory predicted that the confinement of a nanoparticle by the entanglements trapped in the polymer network is softer than that by permanent cross-links and the hopping energy barrier depends linearly on the particle size when entanglements dominate, which is weaker than the quadratic dependence when cross-links dominate. The Dell-Schweizer theory did not distinguish entanglements from cross-links and predicted that the hopping energy barrier asymptotically depends on the particle volume or is proportional to a cubic term of the particle size.

The two qualitatively different theoretical formulations of nanoparticle hopping in cross-linked polymer network have been recently evaluated against the systematic simulations by Sorichetti et al.[122] The detailed evaluation demonstrated that both theories described well the long-time diffusivity of hopping nanoparticles but did not capture well the heterogeneous nanoparticle dynamics at intermediate time scales.

The research on nanoparticle hopping diffusion in cross-linked polymer networks may be extended to glass forming polymer network, an cutting-edge research topic with applications such as separation membranes, barrier materials, and nanofiltration as the technological background. A recent joint theory-experiment-simulation study[193] on the diffusion of large aromatic molecules ("penetrants") in dense cross-linked polymer networks demonstrated that the motion of the penetrants is primarily determined by the coupling of local penetrant hopping to polymer structural relaxation, with the entropic mesh confinement effects being of secondary importance. More aspects of nanoparticle hopping in cross-linked networks have been revealed by molecular simulations. Recent simulations by Dai et al.[104] demonstrated the effects of network topology on hopping diffusion, a timely research direction commensurate with the advances in chemical synthesis that can precisely control the topology of a cross-linked network.[194] Additionally, using molecular simulations and theoretical analysis, Xu et al.[195] have shown more evident nanoparticle hopping diffusion in semiflexible polymer networks. For moderate rigidity, the hopping energy barrier approximately depends linearly on the confinement parameter, which is the ratio of the particle diameter and the network mesh size, in contrast to the quadratic-dependence when network strands are softer and harder. Other than network topology and network strand stiffness, the new physics regarding nanoparticle hopping in a cross-linked polymer network may be further enriched with the use of reversible cross-links, which would introduce a dependence of nanoparticle−polymer coupling on the lifetime of reversible cross-links.

https://doi.org/10.1021/acs.macromol.3c00260
Macromolecules 2023, 56, 3809−3837

II. Many experiments of nanoparticle dynamics are performed in a polymer solution rather than a solvent-free melt. At length scales below the correlation length in a concentrated polymer solution, a nanoparticle is coupled to the solvent viscosity. Above the correlation length, a scaling theory may be developed by renormalizing the corresponding theory for nanoparticles in a polymer melt, as in the pioneering work by Cai et al.[87] The same scaling approach has been used by Cai et al.[88] to describe nanoparticle dynamics in an unentangled polymer gel, which is a mixture of cross-linked unentangled polymer chains and solvent molecules. Similar to nanoparticles in entangled polymer melts and solvent-free cross-linked polymer networks, the ratio of nanoparticle size and the network mesh size has been identified as a key player in the diffusion of nanoparticles in gels.[36,196−199] In addition to the effects of network confinement, various aspects of the interplay between nanoparticles and gel networks, including the effects of network heterogeneity,[36] the nanoscale structural evolution during gelation,[196] controlled defects as in degradable gels, as well as the shape anisotropy of nanoparticles,[199] have been studied in recent experiments. Motivations of studying nanoparticle transport in gels also arise from biological systems. One example is nanoscale transport in biological gel that serves as a barrier against invading pathogens and foreign materials.[200] Another example is vesicle transport in extracellular matrix for the cell−cell communication over long distances.[201]

III. A polymer matrix may be composed of polyelectrolytes and thus bring in electrostatic interactions into the coupling between nanoparticles and polymers. The viscoelasticity of a polyelectrolyte matrix depends on the charge patterns of the polyelectrolyte chains as well as the pH and salt concentrations.[163,202] As a result, the dependencies may be inherited in the coupling between nanoparticles and polyelectrolytes and present themselves as pieces of new physics. In addition, nanoparticles may be charged as well and interact with the polyelectrolytes directly. Rumyantsev et al.[203] recently developed a scaling theory for the structure and dynamics of complex coacervates formed from linear polyelectrolyte chains and oppositely charged spherical colloids, which may represent globular proteins, solid nanoparticles, or spherical micelles of ionic surfactants. The diffusion coefficients of the colloids were predicted to be strongly decreasing functions of the particle size and the charge carried by the particle. The predictions of the scaling theory were compared with the experiments of the coacervation between supercationic globular green fluorescent proteins (GFPs) and anionic RNA, which showed that GFP charge is a key determinant of the protein diffusion in the condensed phase. One more example is the transport of charged particles in biological gels with charged polymers. Charged particles with sizes markedly smaller than the gel network mesh size are often immobilized due to the electrostatic traps, in stark contrast to the high mobility of charge neutral particles of the same size.[200]

Historically, the random motion of particles suspended in a medium was first described in 1827 by Brown, who looked through a microscope at pollens in water. Einstein's 1905 paper and Smoluchowski's 1906 paper with different derivations demonstrated that the Brownian motion of particles of observable dimensions in a fluid reflects the random motion of surrounding fluid atoms, making critical contributions to the establishment of modern atomism. Langevin's 1908 paper constructed a theoretical framework to describe the Brownian motion as being subjected to a deterministic force arising from the fluid viscosity and a fluctuating random force. The theoretical language invented by the pioneers in the early 20th century persists in the 21st century's research on the dynamics of nanoparticles in polymer matrices. The new theoretical approach based on the scaling concepts in polymer physics was initiated in the 2003 paper by Brochard-Wyart and de Gennes[8] and extensively used by Rubinstein and his collaborators.[87,88,101,147] The scaling theory is particularly well-positioned to identify the important length and time scales in an insightful way. Meanwhile, microscopic theories for nanoparticle dynamics in polymer matrices that combine statistical mechanics and polymer physics were developed by Schweizer and his collaborators.[89,90,100,204,205] The microscopic theories have mainly focused on spherical nanoparticles in various polymer matrices but may be potentially expanded to capture the diversity in the nanoparticle−polymer coupling physics as reviewed in this article. Molecular simulation, which was invented in the second half of the 20th century but has already been established as an unparalleled tool complementing experiments and traditional theoretical approaches, has contributed significantly to the research on the dynamics of nanoparticles in polymer matrices. Standard models in coarse-grained nanoparticle−polymer simulations have been developed and calibrated. Looking forward, the development of scale-bridging simulation methods that combine the strengths of fully atomistic and coarse-grained models may help elucidate more pieces of the rich physics in the nanoparticle−polymer coupling. In the age when artificial intelligence permeates to every corner of the world, the rich parameter space for controlling nanoparticle dynamics in polymers would also motivate data scientists to employ machine learning techniques to make data-driven research progress.

Diffusion is the macroscopic manifestation of the microscopic Brownian motion. As the diffusion of nanoparticles in a macromolecular environment is present in many technological applications, such as nanoparticle self-assembly in functional polymer nanocomposites, nanoparticle-based targeted drug and gene delivery, the research on the nanoparticle dynamics dictated by the length- and time-scale dependent coupling between nanoparticles and polymers is anticipated to impact many nanotechnologies, with the potential transformation of the spatial and temporal manipulation of nanoparticles. Furthermore, the research on nanoparticle−polymer coupling may shed light on the transport of bionanoparticles, such as viral nanoparticles, in a complex biological setting[206] and thus broaden its impact in the postpandemic era. It is hoped that the scaling perspective offered in this article based on theoretical and computational research may spur the integration of experiments, simulations, and theory and make impactful progress in the field.

AUTHOR INFORMATION

Corresponding Author

Ting Ge − *Department of Chemistry and Biochemistry, University of South Carolina, Columbia, South Carolina 29208, United States;* orcid.org/0000-0003-2456-732X; Email: tingg@mailbox.sc.edu

Complete contact information is available at: https://pubs.acs.org/10.1021/acs.macromol.3c00260

Notes

The author declares no competing financial interest.

https://doi.org/10.1021/acs.macromol.3c00260
Macromolecules 2023, 56, 3809−3837

Biography

Ting Ge graduated from the University of Science and Technology of China with B. S. in 2007. He received his Ph.D. in Physics from Johns Hopkins University in 2013, under the supervision of the late Prof. Mark O. Robbins. Subsequently, he worked as a postdoctoral researcher in the Research Triangle of North Carolina, first at UNC-Chapel Hill and then at Duke University, supervised both by Prof. Michael Rubinstein. He joined the Department of Chemistry and Biochemistry faculty at the University of South Carolina as an assistant professor in January 2020. He is interested in investigating the microscopic origin of the macroscopic behavior of various polymer and soft matter systems. A combination of molecular simulations and theory is employed in his research activities. Topics currently investigated include (1) the effects of polymer topology on the thermodynamics, rheology, and mechanics of polymeric materials, (2) the transport of nanoscale objects in complex polymeric environments, as well as (3) the scale-bridging physics in the large deformation and fracture behavior of thermoplastics, elastomers, and gels. He has been recognized with the CAREER award from the National Science Foundation.

■ ACKNOWLEDGMENTS

T.G. is grateful to M. Rubinstein and G. S. Grest for the comments on this Perspective. T.G. would like to thank S. Paniukov, D. Vlassopoulos, T. P. Lodge, S. K. Kumar, B. C. Benicewicz, K. I. Winey, R. Composto, R. Leheny, R. Riggleman, K. S. Schweizer, P. Olmsted, E. Kumacheva, L.-H. Cai, S.-W. Cheng, C. Aponte-Rivera, S.-F. Cheng, T. C. O'Connor, J. Wang, J. Clemmer, and P. A. Taylor for discussions and communications regarding this topic at different occasions. S. Zhang and A. Wijesekera helped with the survey of experiments. T.G. acknowledges start-up funds from the University of South Carolina. This work was supported in part by the National Science Foundation EPSCoR Program under NSF Award No.OIA-1655740. Any opinions, findings, and conclusions or recommendations expressed in this material are those of the authors and do not necessarily reflect those of the National Science Foundation. This work is partially supported by an ASPIRE grant from the Office of the Vice President for Research at the University of South Carolina.

■ REFERENCES

(1) Bailey, E. J.; Winey, K. I. Dynamics of polymer segments, polymer chains, and nanoparticles in polymer nanocomposite melts: A review. *Prog. Polym. Sci.* **2020**, *105*, 101242.
(2) Mason, T. G.; Weitz, D. A. Optical measurements of frequency-dependent linear viscoelastic moduli of complex fluids. *Phys. Rev. Lett.* **1995**, *74*, 1250−1253.
(3) Mackintosh, F. C.; Schmidt, C. F. Microrheology. *Curr. Opin. Colloid Interface Sci.* **1999**, *4*, 300−307.
(4) Suk, J. S.; Suh, J.; Choy, K.; Lai, S. K.; Fu, J.; Hanes, J. Gene delivery to differentiated neurotypic cells with RGD and HIV Tat peptide functionalized polymeric nanoparticles. *Biomaterials* **2006**, *27*, 5143−5150.
(5) Lai, S. K.; Wang, Y. Y.; Hanes, J. Mucus-penetrating nanoparticles for drug and gene delivery to mucosal tissues. *Adv. Drug Delivery Rev.* **2009**, *61*, 158−171.
(6) Blanco, E.; Shen, H.; Ferrari, M. Principles of nanoparticle design for overcoming biological barriers to drug delivery. *Nat. Biotechnol.* **2015**, *33*, 941−951.
(7) Bian, X.; Kim, C.; Karniadakis, G. E. 111 years of Brownian motion. *Soft Matter* **2016**, *12*, 6331−6346.
(8) Brochard Wyart, F.; de Gennes, P.-G. Viscosity at small scales in polymer melts. *Eur. Phys. J. E* **2000**, *1*, 93−97.
(9) Doi, M.; Edwards, S. F. *The Theory of Polymer Dynamics*; Oxford University Press: Oxford, U.K., 1988.
(10) Saxton, M. J. Wanted: A positive control for anomalous subdiffusion. *Biophys. J.* **2012**, *103*, 2411−2422.
(11) Guo, H.; Bourret, G.; Lennox, R. B.; Sutton, M.; Harden, J. L.; Leheny, R. L. Entanglement-controlled subdiffusion of nanoparticles within concentrated polymer solutions. *Phys. Rev. Lett.* **2012**, *109*, 1−5.
(12) Kohli, I.; Mukhopadhyay, A. Diffusion of nanoparticles in semidilute polymer solutions: Effect of different length scales. *Macromolecules* **2012**, *45*, 6143−6149.
(13) Schuster, B. S.; Suk, J. S.; Woodworth, G. F.; Hanes, J. Nanoparticle diffusion in respiratory mucus from humans without lung disease. *Biomaterials* **2013**, *34*, 3439−3446.
(14) Kohli, I.; Alam, S.; Patel, B.; Mukhopadhyay, A. Interaction and diffusion of gold nanoparticles in bovine serum albumin solutions. *Appl. Phys. Lett.* **2013**, *102*, 203705.
(15) Chhetri, R. K.; Blackmon, R. L.; Wu, W.-C.; Hill, D. B.; Button, B.; Casbas-Hernandez, P.; Troester, M. A.; Tracy, J. B.; Oldenburg, A. L. Probing biological nanotopology via diffusion of weakly constrained plasmonic nanorods with optical coherence tomography. *Proc. Natl. Acad. Sci. U.S.A.* **2014**, *111*, E4289−E4297.
(16) Babaye Khorasani, F.; Poling-Skutvik, R.; Krishnamoorti, R.; Conrad, J. C. Mobility of nanoparticles in semidilute polyelectrolyte solutions. *Macromolecules* **2014**, *47*, 5328−5333.
(17) Jee, A. Y.; Curtis-Fisk, J. L.; Granick, S. Nanoparticle diffusion in methycellulose thermoreversible association polymer. *Macromolecules* **2014**, *47*, 5793−5797.
(18) de Kort, D. W.; van Duynhoven, J. P. M.; Hoeben, F. J. M.; Janssen, H. M.; Van As, H. NMR nanoparticle diffusometry in hydrogels: Enhancing sensitivity and selectivity. *Anal. Chem.* **2014**, *86*, 9229−9235.
(19) Grabowski, C. A.; Mukhopadhyay, A. Size effect of nanoparticle diffusion in a polymer melt. *Macromolecules* **2014**, *47*, 7238−7242.
(20) Alam, S.; Mukhopadhyay, A. Translational and rotational diffusions of nanorods within semidilute and entangled polymer solutions. *Macromolecules* **2014**, *47*, 6919−6924.
(21) de Kort, D. W.; van Duynhoven, J. P.; VanAs, H.; Mariette, F. Nanoparticle diffusometry for quantitative assessment of submicron structure in food biopolymer networks. *Trends in Food Science and Technology* **2015**, *42*, 13−26.
(22) Poling-Skutvik, R.; Krishnamoorti, R.; Conrad, J. C. Size-Dependent Dynamics of Nanoparticles in Unentangled Polyelectrolyte Solutions. *ACS Macro Lett.* **2015**, *4*, 1169−1173.
(23) de Kort, D. W.; Rombouts, W. H.; Hoeben, F. J. M.; Janssen, H. M.; Van As, H.; van Duynhoven, J. P. M. Scaling Behavior of Dendritic Nanoparticle Mobility in Semidilute Polymer Solutions. *Macromolecules* **2015**, *48*, 7585−7591.
(24) Vagias, A.; Schultze, J.; Doroshenko, M.; Koynov, K.; Butt, H. J.; Gauthier, M.; Fytas, G.; Vlassopoulos, D. Molecular Tracer Diffusion in Nondilute Polymer Solutions: Universal Master Curve and Glass Transition Effects. *Macromolecules* **2015**, *48*, 8907−8912.
(25) Waigh, T. A. Advances in the microrheology of complex fluids. *Rep. Prog. Phys.* **2016**, *79*, 074601.

https://doi.org/10.1021/acs.macromol.3c00260
Macromolecules 2023, 56, 3809−3837

(26) Mangal, R.; Srivastava, S.; Narayanan, S.; Archer, L. A. Size-Dependent Particle Dynamics in Entangled Polymer Nanocomposites. *Langmuir* **2016**, *32*, 596−603.
(27) Lungova, M.; Krutyeva, M.; Pyckhout-Hintzen, W.; Wischnewski, A.; Monkenbusch, M.; Allgaier, J.; Ohl, M.; Sharp, M.; Richter, D. Nanoscale Motion of Soft Nanoparticles in Unentangled and Entangled Polymer Matrices. *Phys. Rev. Lett.* **2016**, *117*, 1−5.
(28) Gupta, S.; Biehl, R.; Sill, C.; Allgaier, J.; Sharp, M.; Ohl, M.; Richter, D. Protein Entrapment in Polymeric Mesh: Diffusion in Crowded Environment with Fast Process on Short Scales. *Macromolecules* **2016**, *49*, 1941−1949.
(29) Mangal, R.; Wen, Y. H.; Choudhury, S.; Archer, L. A. Multiscale Dynamics of Polymers in Particle-Rich Nanocomposites. *Macromolecules* **2016**, *49*, 5202−5212.
(30) Griffin, P. J.; Bocharova, V.; Middleton, L. R.; Composto, R. J.; Clarke, N.; Schweizer, K. S.; Winey, K. I. Influence of the Bound Polymer Layer on Nanoparticle Diffusion in Polymer Melts. *ACS Macro Lett.* **2016**, *5*, 1141−1145.
(31) Maldonado-Camargo, L.; Rinaldi, C. Breakdown of the Stokes-Einstein Relation for the Rotational Diffusivity of Polymer Grafted Nanoparticles in Polymer Melts. *Nano Lett.* **2016**, *16*, 6767−6773.
(32) Witten, J.; Ribbeck, K. The particle in the spider's web: Transport through biological hydrogels. *Nanoscale* **2017**, *9*, 8080−8095.
(33) Shokeen, N.; Issa, C.; Mukhopadhyay, A. Comparison of nanoparticle diffusion using fluorescence correlation spectroscopy and differential dynamic microscopy within concentrated polymer solutions. *Appl. Phys. Lett.* **2017**, *111*, 263703.
(34) Senses, E.; Ansar, S. M.; Kitchens, C. L.; Mao, Y.; Narayanan, S.; Natarajan, B.; Faraone, A. Small Particle Driven Chain Disentanglements in Polymer Nanocomposites. *Phys. Rev. Lett.* **2017**, *118*, 1−5.
(35) Schuster, B. S.; Allan, D. B.; Kays, J. C.; Hanes, J.; Leheny, R. L. Photoactivatable fluorescent probes reveal heterogeneous nanoparticle permeation through biological gels at multiple scales. *J. Controlled Release* **2017**, *260*, 124−133.
(36) Parrish, E.; Caporizzo, M. A.; Composto, R. J. Network confinement and heterogeneity slows nanoparticle diffusion in polymer gels. *J. Chem. Phys.* **2017**, *146*, 203318.
(37) Maldonado-Camargo, L.; Yang, C.; Rinaldi, C. Scale-dependent rotational diffusion of nanoparticles in polymer solutions. *Nanoscale* **2017**, *9*, 12039−12050.
(38) Lin, C. C.; Griffin, P. J.; Chao, H.; Hore, M. J.; Ohno, K.; Clarke, N.; Riggleman, R. A.; Winey, K. I.; Composto, R. J. Grafted polymer chains suppress nanoparticle diffusion in athermal polymer melts. *J. Chem. Phys.* **2017**, *146*, 203332.
(39) Lee, J.; Grein-Iankovski, A.; Narayanan, S.; Leheny, R. L. Nanorod mobility within entangled wormlike micelle solutions. *Macromolecules* **2017**, *50*, 406−415.
(40) Cheng, S.; Xie, S. J.; Carrillo, J. M. Y.; Carroll, B.; Martin, H.; Cao, P. F.; Dadmun, M. D.; Sumpter, B. G.; Novikov, V. N.; Schweizer, K. S.; Sokolov, A. P. Big Effect of Small Nanoparticles: A Shift in Paradigm for Polymer Nanocomposites. *ACS Nano* **2017**, *11*, 752−759.
(41) Ramani, M.; Mudge, M. C.; Morris, R. T.; Zhang, Y.; Warcholek, S. A.; Hurst, M. N.; Riviere, J. E.; DeLong, R. K. Zinc Oxide Nanoparticle-Poly I:C RNA Complexes: Implication as Therapeutics against Experimental Melanoma. *Mol. Pharmaceutics* **2017**, *14*, 614−625.
(42) Vagias, A.; Sergelen, K.; Koynov, K.; Košovan, P.; Dostalek, J.; Jonas, U.; Knoll, W.; Fytas, G. Diffusion and Permeation of Labeled IgG in Grafted Hydrogels. *Macromolecules* **2017**, *50*, 4770−4779.
(43) Johnson, K. J.; Glynos, E.; Maroulas, S. D.; Narayanan, S.; Sakellariou, G.; Green, P. F. Confinement Effects on Host Chain Dynamics in Polymer Nanocomposite Thin Films. *Macromolecules* **2017**, *50*, 7241−7248.
(44) Nath, P.; Mangal, R.; Kohle, F.; Choudhury, S.; Narayanan, S.; Wiesner, U.; Archer, L. A. Dynamics of Nanoparticles in Entangled Polymer Solutions. *Langmuir* **2018**, *34*, 241−249.
(45) Molaei, M.; Atefi, E.; Crocker, J. C. Nanoscale Rheology and Anisotropic Diffusion Using Single Gold Nanorod Probes. *Phys. Rev. Lett.* **2018**, *120*, 118002.
(46) Hong, W.; Xu, G.; Ou, X.; Sun, W.; Wang, T.; Tong, Z. Colloidal probe dynamics in gelatin solution during the sol-gel transition. *Soft Matter* **2018**, *14*, 3694−3703.
(47) Poling-Skutvik, R.; Lee, J.; Narayanan, S.; Krishnamoorti, R.; Conrad, J. C. Tunable Assembly of Gold Nanorods in Polymer Solutions to Generate Controlled Nanostructured Materials. *ACS Applied Nano Materials* **2018**, *1*, 877−885.
(48) Carroll, B.; Bocharova, V.; Carrillo, J. M. Y.; Kisliuk, A.; Cheng, S.; Yamamoto, U.; Schweizer, K. S.; Sumpter, B. G.; Sokolov, A. P. Diffusion of Sticky Nanoparticles in a Polymer Melt: Crossover from Suppressed to Enhanced Transport. *Macromolecules* **2018**, *51*, 2268−2275.
(49) Song, J. J.; Bhattacharya, R.; Kim, H.; Chang, J.; Tang, T. Y.; Guo, H.; Ghosh, S. K.; Yang, Y.; Jiang, Z.; Kim, H.; Russell, T. P.; Arya, G.; Narayanan, S.; Sinha, S. K. One-Dimensional Anomalous Diffusion of Gold Nanoparticles in a Polymer Melt. *Phys. Rev. Lett.* **2019**, *122*, 107802.
(50) Senanayake, K. K.; Shokeen, N.; Fakhrabadi, E. A.; Liberatore, M. W.; Mukhopadhyay, A. Diffusion of nanoparticles within a semidilute polyelectrolyte solution. *Soft Matter* **2019**, *15*, 7616−7622.
(51) Hess, M.; Roeben, E.; Habicht, A.; Seiffert, S.; Schmidt, A. M. Local dynamics in supramolecular polymer networks probed by magnetic particle nanorheology. *Soft Matter* **2019**, *15*, 842−850.
(52) Hess, M.; Roeben, E.; Rochels, P.; Zylla, M.; Webers, S.; Wende, H.; Schmidt, A. M. Size effects on rotational particle diffusion in complex fluids as probed by Magnetic Particle Nanorheology. *Phys. Chem. Chem. Phys.* **2019**, *21*, 26525−26539.
(53) Cherstvy, A. G.; Thapa, S.; Wagner, C. E.; Metzler, R. Non-Gaussian, non-ergodic, and non-Fickian diffusion of tracers in mucin hydrogels. *Soft Matter* **2019**, *15*, 2526−2551.
(54) Chen, R.; Poling-Skutvik, R.; Howard, M. P.; Nikoubashman, A.; Egorov, S. A.; Conrad, J. C.; Palmer, J. C. Influence of polymer flexibility on nanoparticle dynamics in semidilute solutions. *Soft Matter* **2019**, *15*, 1260−1268.
(55) Senanayake, K. K.; Fakhrabadi, E. A.; Liberatore, M. W.; Mukhopadhyay, A. Diffusion of Nanoparticles in Entangled Poly(vinyl alcohol) Solutions and Gels. *Macromolecules* **2019**, *52*, 787−795.
(56) Senanayake, K. K.; Mukhopadhyay, A. Nanoparticle Diffusion within Dilute and Semidilute Xanthan Solutions. *Langmuir* **2019**, *35*, 7978−7984.
(57) Poling-Skutvik, R.; Slim, A. H.; Narayanan, S.; Conrad, J. C.; Krishnamoorti, R. Soft interactions modify the diffusive dynamics of polymer-grafted nanoparticles in solutions of free polymer. *ACS Macro Lett.* **2019**, *8*, 917−922.
(58) Gratz, M.; Tschöpe, A. Size Effects in the Oscillatory Rotation Dynamics of Ni Nanorods in Poly(ethylene oxide) Solutions. *Macromolecules* **2019**, *52*, 6600−6612.
(59) Mansel, B. W.; Chen, C. Y.; Lin, J. M.; Huang, Y. S.; Lin, Y. C.; Chen, H. L. Hierarchical Structure and Dynamics of a Polymer/Nanoparticle Hybrid Displaying Attractive Polymer-Particle Interaction. *Macromolecules* **2019**, *52*, 8741−8750.
(60) You, W.; Yu, W. Slow Linear Viscoelastic Relaxation of Polymer Nanocomposites: Contribution from Confined Diffusion of Nanoparticles. *Macromolecules* **2019**, *52*, 9094−9104.
(61) Yang, S. G.; Xie, H. J.; Saba, H.; Cseh, L.; Ungar, G. Fluorescence microscopy tracking of dyes, nanoparticles and quantum dots during growth of polymer spherulites. *Polymer* **2020**, *191*, 122246.
(62) Rose, K. A.; Molaei, M.; Boyle, M. J.; Lee, D.; Crocker, J. C.; Composto, R. J. Particle tracking of nanoparticles in soft matter. *J. Appl. Phys.* **2020**, *127*, 191101.
(63) Kanduč, M.; Kim, W. K.; Roa, R.; Dzubiella, J. Modeling of stimuli-responsive nanoreactors: Rational rate control towards the design of colloidal enzymes. *Molecular Systems Design and Engineering* **2020**, *5*, 602−619.
(64) Hess, M.; Gratz, M.; Remmer, H.; Webers, S.; Landers, J.; Borin, D.; Ludwig, F.; Wende, H.; Odenbach, S.; Tschöpe, A.; Schmidt, A. M. Scale-dependent particle diffusivity and apparent viscosity in polymer solutions as probed by dynamic magnetic nanorheology. *Soft Matter* **2020**, *16*, 7562−7575.

https://doi.org/10.1021/acs.macromol.3c00260
Macromolecules 2023, 56, 3809−3837

(65) Rodríguez-Suárez, J. M.; Butler, C. S.; Gershenson, A.; Lau, B. L. Heterogeneous Diffusion of Polystyrene Nanoparticles through an Alginate Matrix: The Role of Cross-linking and Particle Size. *Environ. Sci. Technol.* **2020**, *54*, 5159−5166.
(66) Xue, C.; Shi, X.; Tian, Y.; Zheng, X.; Hu, G. Diffusion of nanoparticles with activated hopping in crowded polymer solutions. *Nano Lett.* **2020**, *20*, 3895−3904.
(67) Park, J.; Bailey, E. J.; Composto, R. J.; Winey, K. I. Single-Particle Tracking of Nonsticky and Sticky Nanoparticles in Polymer Melts. *Macromolecules* **2020**, *53*, 3933−3939.
(68) Slim, A. H.; Poling-Skutvik, R.; Conrad, J. C. Local Confinement Controls Diffusive Nanoparticle Dynamics in Semidilute Polyelectrolyte Solutions. *Langmuir* **2020**, *36*, 9153−9159.
(69) Shrestha, U. M.; Han, L.; Saito, T.; Schweizer, K. S.; Dadmun, M. D. Mechanism of Soft Nanoparticle Diffusion in Entangled Polymer Melts. *Macromolecules* **2020**, *53*, 7580−7589.
(70) Wu, D.; Weiblen, D. G.; Ozisik, R.; Akcora, P. Local Viscosity of Interfacial Layers in Polymer Nanocomposites Measured by Magnetic Heating. *ACS Applied Polymer Materials* **2020**, *2*, 5542−5549.
(71) Unni, M.; Savliwala, S.; Partain, B. D.; Maldonado-Camargo, L.; Zhang, Q.; Narayanan, S.; Dufresne, E. M.; Ilavsky, J.; Grybos, P.; Koziol, A.; Maj, P.; Szczygiel, R.; Allen, K. D.; Rinaldi-Ramos, C. M. Fast nanoparticle rotational and translational diffusion in synovial fluid and hyaluronic acid solutions. *Science Advances* **2021**, *7*, 1−14.
(72) Espasa-Valdepeñas, A.; Vega, J. F.; Cruz, V.; Ramos, J.; Müller, A. J.; Martinez-Salazar, J. Revisiting Polymer-Particle Interaction in PEO Solutions. *Langmuir* **2021**, *37*, 3808−3816.
(73) Smith, M.; Poling-Skutvik, R.; Slim, A. H.; Willson, R. C.; Conrad, J. C. Dynamics of Flexible Viruses in Polymer Solutions. *Macromolecules* **2021**, *54*, 4557−4563.
(74) Yavitt, B. M.; Salatto, D.; Zhou, Y.; Huang, Z.; Endoh, M.; Wiegart, L.; Bocharova, V.; Ribbe, A. E.; Sokolov, A. P.; Schweizer, K. S.; Koga, T. Collective Nanoparticle Dynamics Associated with Bridging Network Formation in Model Polymer Nanocomposites. *ACS Nano* **2021**, *15*, 11501−11513.
(75) Nikitin, A. A.; Yurenya, A. Y.; Gabbasov, R. R.; Cherepanov, V. M.; Polikarpov, M. A.; Chuev, M. A.; Majouga, A. G.; Panchenko, V. Y.; Abakumov, M. A. Effects of Macromolecular Crowding on Nanoparticle Diffusion: New Insights from Mössbauer Spectroscopy. *J. Phys. Chem. Lett.* **2021**, *12*, 6804−6811.
(76) Mao, Y.; Nielsen, P.; Ali, J. Passive and Active Microrheology for Biomedical Systems. *Frontiers in Bioengineering and Biotechnology* **2022**, *10*, 916354.
(77) Langevin, D. Motion of small bubbles and drops in viscoelastic fluids. *Curr. Opin. Colloid Interface Sci.* **2022**, *57*, 101529.
(78) Moncure, P. J.; Simon, Z. C.; Millstone, J. E.; Laaser, J. E. Relationship between Gel Mesh and Particle Size in Determining Nanoparticle Diffusion in Hydrogel Nanocomposites. *J. Phys. Chem. B* **2022**, *126*, 4132−4142.
(79) Calabrese, V.; Varchanis, S.; Haward, S. J.; Shen, A. Q. Alignment of Colloidal Rods in Crowded Environments. *Macromolecules* **2022**, *55*, 5610−5620.
(80) Suwa, M.; Uotani, A.; Tojo, Y.; Onodera, R.; Tsukahara, S. Orientational Dynamics of Magnetic Iron Oxide Nanoparticles in a Hydrogel: Observation by Magnetic Linear Dichroism under Oscillating Field. *Langmuir* **2022**, *38*, 9708−9719.
(81) Wang, K.; Composto, R. J.; Winey, K. I. ToF-SIMS Depth Profiling to Measure Nanoparticle and Polymer Diffusion in Polymer Melts. *Macromolecules* **2023**, *56*, 2277−2285.
(82) Qiang, Z.; Wang, M. 100th anniversary of macromolecular science viewpoint: Enabling advances in fluorescence microscopy techniques. *ACS Macro Lett.* **2020**, *9*, 1342−1356.
(83) Kalathi, J. T.; Grest, G. S.; Kumar, S. K. Universal viscosity behavior of polymer nanocomposites. *Phys. Rev. Lett.* **2012**, *109*, 198301.
(84) Lin, C. C.; Parrish, E.; Composto, R. J. Macromolecule and Particle Dynamics in Confined Media. *Macromolecules* **2016**, *49*, 5755−5772.
(85) Senses, E.; Kitchens, C. L.; Faraone, A. Viscosity reduction in polymer nanocomposites: Insights from dynamic neutron and X-ray scattering. *J. Polym. Sci.* **2022**, *60*, 1130−1150.
(86) Boyle, M. J.; Maguire, S. M.; Rose, K. A.; Lee, D.; Composto, R. J. Nanoparticle Transport Through Polymers and Along Interfaces. *Macromolecular Engineering: From Precise Synthesis to Macroscopic Materials and Applications*; John Wiley & Sons, Ltd.: Hoboken, NJ, 2022.
(87) Cai, L.-H.; Panyukov, S.; Rubinstein, M. Mobility of Nonsticky Nanoparticles in Polymer Liquids. *Macromolecules* **2011**, *44*, 7853−7863.
(88) Cai, L. H.; Panyukov, S.; Rubinstein, M. Hopping diffusion of nanoparticles in polymer matrices. *Macromolecules* **2015**, *48*, 847−862.
(89) Dell, Z. E.; Schweizer, K. S. Theory of localization and activated hopping of nanoparticles in cross-linked networks and entangled polymer melts. *Macromolecules* **2014**, *47*, 405−414.
(90) Yamamoto, U.; Schweizer, K. S. Microscopic theory of the long-time diffusivity and intermediate-time anomalous transport of a nanoparticle in polymer melts. *Macromolecules* **2015**, *48*, 152−163.
(91) Thompson, A. P.; Aktulga, H. M.; Berger, R.; Bolintineanu, D. S.; Brown, W. M.; Crozier, P. S.; in 't Veld, P. J.; Kohlmeyer, A.; Moore, S. G.; Nguyen, T. D.; Shan, R.; Stevens, M. J.; Tranchida, J.; Trott, C.; Plimpton, S. J. LAMMPS-a flexible simulation tool for particle-based materials modeling at the atomic, meso, and continuum scales. *Comput. Phys. Commun.* **2022**, *271*, 108171.
(92) Kremer, K.; Grest, G. S. Dynamics of entangled linear polymer melts: A molecular dynamics simulation. *J. Chem. Phys.* **1990**, *92*, 5057−5086.
(93) Everaers, R.; Karimi-Varzaneh, H. A.; Fleck, F.; Hojdis, N.; Svaneborg, C. Kremer−Grest Models for Commodity Polymer Melts: Linking Theory, Experiment, and Simulation at the Kuhn Scale. *Macromolecules* **2020**, *53*, 1901−1916.
(94) Karim, M.; Kohale, S. C.; Indei, T.; Schieber, J. D.; Khare, R. Determination of viscoelastic properties by analysis of probe-particle motion in molecular simulations. *Physical Review E - Statistical, Nonlinear, and Soft Matter Physics* **2012**, *86*, 1−6.
(95) Karim, M.; Indei, T.; Schieber, J. D.; Khare, R. Determination of linear viscoelastic properties of an entangled polymer melt by probe rheology simulations. *Phys. Rev. E* **2016**, *93*, 1−12.
(96) Wang, J.; O'Connor, T. C.; Grest, G. S.; Zheng, Y.; Rubinstein, M.; Ge, T. Diffusion of Thin Nanorods in Polymer Melts. *Macromolecules* **2021**, *54*, 7051−7059.
(97) Zhang, S.; Wang, J.; Ge, T. Force-driven active dynamics of thin nanorods in unentangled polymer melts. *Soft Matter* **2022**, *18*, 6582−6591.
(98) Everaers, R.; Ejtehadi, M. R. Interaction potentials for soft and hard ellipsoids. *Phys. Rev. E* **2003**, *67*, 041710.
(99) Monti, J. M.; Clemmer, J. T.; Srivastava, I.; Silbert, L. E.; Grest, G. S.; Lechman, J. B. Large-scale frictionless jamming with power-law particle size distributions. *Phys. Rev. E* **2022**, *106*, 1−13.
(100) Kalathi, J. T.; Yamamoto, U.; Schweizer, K. S.; Grest, G. S.; Kumar, S. K. Nanoparticle diffusion in polymer nanocomposites. *Phys. Rev. Lett.* **2014**, *112*, 108301.
(101) Ge, T.; Kalathi, J. T.; Halverson, J. D.; Grest, G. S.; Rubinstein, M. Nanoparticle Motion in Entangled Melts of Linear and Nonconcatenated Ring Polymers. *Macromolecules* **2017**, *50*, 1749−1754.
(102) Ge, T.; Grest, G. S.; Rubinstein, M. Nanorheology of Entangled Polymer Melts. *Phys. Rev. Lett.* **2018**, *120*, 57801.
(103) Ge, T.; Rubinstein, M.; Grest, G. S. Effects of Tethered Polymers on Dynamics of Nanoparticles in Unentangled Polymer Melts. *Macromolecules* **2020**, *53*, 6898−6906.
(104) Dai, X.; Zhang, X.; Gao, L.; Xu, Z.; Yan, L. T. Topology mediates transport of nanoparticles in macromolecular networks. *Nat. Commun.* **2022**, *13*, 1−8.
(105) Zhou, X.; Jiang, Y.; Chen, J.; He, L.; Zhang, L. Size-dependent nanoparticle dynamics in semiflexible ring polymer nanocomposites. *Polymer* **2017**, *131*, 243−251.

https://doi.org/10.1021/acs.macromol.3c00260
Macromolecules 2023, 56, 3809−3837

(106) Zhao, B. R.; Li, B. Molecular simulation of hopping mechanisms of nanoparticles in regular cross-linked polymer networks. *J. Chem. Phys.* **2022**, *157*, 104901.
(107) Zhao, B. R.; Li, B.; Shi, X. Molecular simulation of the diffusion mechanism of nanorods in cross-linked networks. *Nanoscale* **2021**, *13*, 17404−17416.
(108) Nourian, P.; Islam, R.; Khare, R. Implementation of active probe rheology simulation technique for determining the viscoelastic moduli of soft matter. *J. Rheol.* **2021**, *65*, 617−632.
(109) Nahali, N.; Rosa, A. Nanoprobe diffusion in entangled polymer solutions: Linear vs. unconcatenated ring chains. *J. Chem. Phys.* **2018**, *148*, 194902.
(110) Lu, Y.; Hu, G. H. A potential barrier in the diffusion of nanoparticles in ordered polymer networks. *Soft Matter* **2021**, *17*, 6374−6382.
(111) Li, S. J.; Qian, H. J.; Lu, Z. Y. Translational and rotational dynamics of an ultra-thin nanorod probe particle in linear polymer melts. *Phys. Chem. Chem. Phys.* **2018**, *20*, 20996−21007.
(112) Kuhnhold, A.; Paul, W. Active one-particle microrheology of an unentangled polymer melt studied by molecular dynamics simulation. *Physical Review E - Statistical, Nonlinear, and Soft Matter Physics* **2015**, *91*, 1−7.
(113) Kuldová, J.; Uhlík, F.; Košovan, P. The drag of the tails: Diffusion of sticky nanoparticles in dilute polymer solutions. *J. Chem. Phys.* **2015**, *143*, 243129.
(114) Kuhnhold, A.; Paul, W. Passive one-particle microrheology of an unentangled polymer melt studied by molecular dynamics simulation. *Physical Review E - Statistical, Nonlinear, and Soft Matter Physics* **2014**, *90*, 1−12.
(115) Karatrantos, A.; Composto, R. J.; Winey, K. I.; Clarke, N. Polymer and spherical nanoparticle diffusion in nanocomposites. *J. Chem. Phys.* **2017**, *146*, 203331.
(116) Jia, X. M.; Qian, H. J.; Lu, Z. Y. The interfacial structure and dynamics in a polymer nanocomposite containing small attractive nanoparticles: A full atomistic molecular dynamics simulation study. *Phys. Chem. Chem. Phys.* **2020**, *22*, 11400−11408.
(117) Chen, Y.; Xu, H.; Ma, Y.; Liu, J.; Zhang, L. Diffusion of polymer-grafted nanoparticles with dynamical fluctuations in unentangled polymer melts. *Phys. Chem. Chem. Phys.* **2022**, *24*, 11322−11335.
(118) Chen, R.; Kotkar, S. B.; Poling-Skutvik, R.; Howard, M. P.; Nikoubashman, A.; Conrad, J. C.; Palmer, J. C. Nanoparticle dynamics in semidilute polymer solutions: Rings versus linear chains. *J. Rheol.* **2021**, *65*, 745−755.
(119) Chen, A.; Zhao, N.; Hou, Z. The effect of hydrodynamic interactions on nanoparticle diffusion in polymer solutions: A multiparticle collision dynamics study. *Soft Matter* **2017**, *13*, 8625−8635.
(120) Cao, X. Z.; Merlitz, H.; Wu, C. X. Tuning Adsorption Duration to Control the Diffusion of a Nanoparticle in Adsorbing Polymers. *J. Phys. Chem. Lett.* **2017**, *8*, 2629−2633.
(121) Sorichetti, V.; Hugouvieux, V.; Kob, W. Structure and Dynamics of a Polymer-Nanoparticle Composite: Effect of Nanoparticle Size and Volume Fraction. *Macromolecules* **2018**, *51*, 5375−5391.
(122) Sorichetti, V.; Hugouvieux, V.; Kob, W. Dynamics of Nanoparticles in Polydisperse Polymer Networks: From Free Diffusion to Hopping. *Macromolecules* **2021**, *54*, 8575−8589.
(123) Ge, T.; Panyukov, S.; Rubinstein, M. Self-Similar Conformations and Dynamics in Entangled Melts and Solutions of Nonconcatenated Ring Polymers. *Macromolecules* **2016**, *49*, 708−722.
(124) Kruteva, M.; Allgaier, J.; Monkenbusch, M.; Porcar, L.; Richter, D. Self-Similar Polymer Ring Conformations Based on Elementary Loops: A Direct Observation by SANS. *ACS Macro Lett.* **2020**, *9*, 507−511.
(125) Kruteva, M.; Monkenbusch, M.; Allgaier, J.; Holderer, O.; Pasini, S.; Hoffmann, I.; Richter, D. Self-Similar Dynamics of Large Polymer Rings: A Neutron Spin Echo Study. *Phys. Rev. Lett.* **2020**, *125*, 238004.
(126) Romio, M.; Trachsel, L.; Morgese, G.; Ramakrishna, S. N.; Spencer, N. D.; Benetti, E. M. Topological Polymer Chemistry Enters Materials Science: Expanding the Applicability of Cyclic Polymers. *ACS Macro Lett.* **2020**, *9*, 1024−1033.
(127) Haque, F. M.; Grayson, S. M. The synthesis, properties and potential applications of cyclic polymers. *Nat. Chem.* **2020**, *12*, 433.
(128) Rubinstein, M.; Colby, R. H. *Polymer Physics*; Oxford University Press: Oxford, U.K., 2003.
(129) Obukhov, S.; Johner, A.; Baschnagel, J.; Meyer, H.; Wittmer, J. P. Melt of polymer rings: The decorated loop model. *Europhys. Lett.* **2014**, *105*, 48005.
(130) Kapnistos, M.; Lang, M.; Vlassopoulos, D.; Pyckhout-Hintzen, W.; Richter, D.; Cho, D.; Chang, T.; Rubinstein, M. Unexpected power-law stress relaxation of entangled ring polymers. *Nat. Mater.* **2008**, *7*, 997−1002.
(131) Parisi, D.; Ahn, J.; Chang, T.; Vlassopoulos, D.; Rubinstein, M. Stress Relaxation in Symmetric Ring-Linear Polymer Blends at Low Ring Fractions. *Macromolecules* **2020**, *53*, 1685−1693.
(132) Peddireddy, K. R.; Lee, M.; Schroeder, C. M.; Robertson-Anderson, R. M. Viscoelastic properties of ring-linear DNA blends exhibit nonmonotonic dependence on blend composition. *Physical Review Research* **2020**, *2*, 023213.
(133) Martin, H. J.; White, B. T.; Scanlon, C. J.; Saito, T.; Dadmun, M. D. Tunable synthetic control of soft polymeric nanoparticle morphology. *Soft Matter* **2017**, *13*, 8849−8857.
(134) Imel, A. E.; Rostom, S.; Holley, W.; Baskaran, D.; Mays, J. W.; Dadmun, M. D. The tracer diffusion coefficient of soft nanoparticles in a linear polymer matrix. *RSC Adv.* **2017**, *7*, 15574−15581.
(135) Rostom, S.; Dadmun, M. D. The impact of nanoparticle softness on its tracer diffusion coefficient in all polymer nanocomposites. *J. Appl. Phys.* **2020**, *127*, 074303.
(136) Li, Z. J.; Chen, X. L.; Li, H. J.; Tu, Q. Y.; Yang, Z.; Xu, Y. P.; Hu, B. Q. Synthesis and Raman scattering of GaN nanorings, nanoribbons and nanowires. *Applied Physics A: Materials Science and Processing* **2001**, *72*, 629−632.
(137) Kong, X. Y.; Ding, Y.; Yang, R.; Wang, Z. L. Single-Crystal Nanorings Formed by Epitaxial Self-Coiling of Polar Nanobelts. *Science* **2004**, *303*, 1348−1351.
(138) Broedersz, C. P.; Mackintosh, F. C. Modeling semiflexible polymer networks. *Rev. Mod. Phys.* **2014**, *86*, 995−1036.
(139) Anderson, S. J.; Matsuda, C.; Garamella, J.; Peddireddy, K. R.; Robertson-Anderson, R. M.; McGorty, R. Filament Rigidity Vies with Mesh Size in Determining Anomalous Diffusion in Cytoskeleton. *Biomacromolecules* **2019**, *20*, 4380−4388.
(140) Sonn-Segev, A.; Bernheim-Groswasser, A.; Diamant, H.; Roichman, Y. Viscoelastic Response of a Complex Fluid at Intermediate Distances. *Phys. Rev. Lett.* **2014**, *112*, 088301.
(141) Tu, M. Q.; Davydovich, O.; Mei, B.; Singh, P. K.; Grest, G. S.; Schweizer, K. S.; O'Connor, T. C.; Schroeder, C. M. Unexpected Slow Relaxation Dynamics in Pure Ring Polymers Arise from Intermolecular Interactions. *ACS Polym. Au* **2023** DOI: 10.1021/acspolymersau.2c00069.
(142) Cai, L. H.; Kodger, T. E.; Guerra, R. E.; Pegoraro, A. F.; Rubinstein, M.; Weitz, D. A. Soft Poly(dimethylsiloxane) Elastomers from Architecture-Driven Entanglement Free Design. *Adv. Mater.* **2015**, *27*, 5132−5140.
(143) Sheiko, S. S.; Dobrynin, A. V. Architectural Code for Rubber Elasticity: From Supersoft to Superfirm Materials. *Macromolecules* **2019**, *52*, 7531−7546.
(144) Chan, J. M.; Kordon, A. C.; Zhang, R.; Wang, M. Direct visualization of bottlebrush polymer conformations in the solid state. *Proc. Natl. Acad. Sci. U.S.A.* **2021**, *118*, 1−9.
(145) Kumar, S. K.; Jouault, N.; Benicewicz, B.; Neely, T. Nanocomposites with polymer grafted nanoparticles. *Macromolecules* **2013**, *46*, 3199−3214.
(146) Kumar, S. K.; Benicewicz, B. C.; Vaia, R. A.; Winey, K. I. 50th Anniversary Perspective: Are Polymer Nanocomposites Practical for Applications? *Macromolecules* **2017**, *50*, 714−731.

(147) Ge, T.; Rubinstein, M. Mobility of Polymer-Tethered Nanoparticles in Unentangled Polymer Melts. *Macromolecules* **2019**, *52*, 1536−1545.
(148) Daoud, M.; Cotton, J. P. Star shaped polymers: a model for the conformation and its concentration dependence. *J. Phys. (Paris)* **1982**, *43*, 531−538.
(149) Raphael, E.; Pincus, P.; Fredrickson, G. H. Conformation of Star Polymers in High Molecular Weight Solvents. *Macromolecules* **1993**, *26*, 1996−2006.
(150) Aubouy, M.; Fredrickson, G. H.; Pincus, P.; Raphaeel, E. End-Tethered Chains in Polymeric Matrices. *Macromolecules* **1995**, *28*, 2979−2981.
(151) Gay, C.; Raphaël, E. Static Properties of a Star Polymer in a High Molecular Weight Solvent. *J. Phys. II* **1996**, *6*, 587−591.
(152) Parisi, D.; Buenning, E.; Kalafatakis, N.; Gury, L.; Benicewicz, B. C.; Gauthier, M.; Cloitre, M.; Rubinstein, M.; Kumar, S. K.; Vlassopoulos, D. Universal Polymeric-to-Colloidal Transition in Melts of Hairy Nanoparticles. *ACS Nano* **2021**, *15*, 16697−16708.
(153) Yamamoto, U.; Carrillo, J. M. Y.; Bocharova, V.; Sokolov, A. P.; Sumpter, B. G.; Schweizer, K. S. Theory and Simulation of Attractive Nanoparticle Transport in Polymer Melts. *Macromolecules* **2018**, *51*, 2258−2267.
(154) Bailey, E. J.; Griffin, P. J.; Composto, R. J.; Winey, K. I. Multiscale Dynamics of Small, Attractive Nanoparticles and Entangled Polymers in Polymer Nanocomposites. *Macromolecules* **2019**, *52*, 2181−2188.
(155) Ge, T.; Grest, G. S.; Rubinstein, M. (manuscript in preparation).
(156) de Gennes, P.-G. Ecoulement viscosimetriques de polymeres enchevetres. *C. R. Acad. Sci. B* **1979**, *288*, 219−220.
(157) Drda, P. P.; Wang, S. Q. Stick-slip transition at polymer melt/solid interfaces. *Phys. Rev. Lett.* **1995**, *75*, 2698−2701.
(158) Brochard-Wyart, F.; Gay, C.; De Gennes, P. G. Slippage of polymer melts on grafted surfaces. *Macromolecules* **1996**, *29*, 377−382.
(159) Brochard, F.; de Gennes, P. G. *Shear-Dependent Slippage at Polymer/Solid Interface W1* **1992**, *8*, 3033−3037.
(160) Einzel, D.; Panzer, P.; Liu, M. Boundary Condition for Fluid Flow: Curved or Rough Surfaces. *Phys. Rev. Lett.* **1990**, *64*, 2269−2272.
(161) Barber, R. W.; Sun, Y.; Gu, X. J.; Emerson, D. R. Isothermal slip flow over curved surfaces. *Vacuum* **2004**, *76*, 73−81.
(162) Hore, M. J.; Composto, R. J. Functional polymer nanocomposites enhanced by nanorods. *Macromolecules* **2014**, *47*, 875−887.
(163) Aponte-Rivera, C.; Rubinstein, M. Dynamic Coupling in Unentangled Liquid Coacervates Formed by Oppositely Charged Polyelectrolytes. *Macromolecules* **2021**, *54*, 1783−1800.
(164) de Gennes, P. G. Motions of one stiff molecule in an entangled polymer melt. *J. Phys. (Paris)* **1981**, *42*, 473−477.
(165) Fakhri, N.; MacKintosh, F. C.; Lounis, B.; Cognet, L.; Pasquali, M. Brownian Motion of Stiff Filaments in a Crowded Environment. *Science* **2010**, *330*, 1804−1807.
(166) Odijk, T. The statistics and dynamics of confined or entangled stiff polymers. *Macromolecules* **1983**, *16*, 1340−1344.
(167) Choi, J.; Cargnello, M.; Murray, C. B.; Clarke, N.; Winey, K. I.; Composto, R. J. Fast Nanorod Diffusion through Entangled Polymer Melts. *ACS Macro Lett.* **2015**, *4*, 952−956.
(168) Lu, S.; Jayaraman, A. Effect of Nanorod Physical Roughness on the Aggregation and Percolation of Nanorods in Polymer Nanocomposites. *ACS Macro Lett.* **2021**, *10*, 1416−1422.
(169) Drake, G. A.; Keating, L. P.; Shim, M. Design Principles of Colloidal Nanorod Heterostructures. *Chem. Rev.* **2023**, *123*, 3761.
(170) Yao, L.; Ou, Z.; Luo, B.; Xu, C.; Chen, Q. Machine Learning to Reveal Nanoparticle Dynamics from Liquid-Phase TEM Videos. *ACS Central Science* **2020**, *6*, 1421−1430.
(171) Choueiri, R. M.; Galati, E.; Thérien-Aubin, H.; Klinkova, A.; Larin, E. M.; Querejeta-Fernández, A.; Han, L.; Xin, H. L.; Gang, O.; Zhulina, E. B.; Rubinstein, M.; Kumacheva, E. Surface patterning of nanoparticles with polymer patches. *Nature* **2016**, *538*, 79−83.
(172) Krook, N. M.; Tabedzki, C.; Elbert, K. C.; Yager, K. G.; Murray, C. B.; Riggleman, R. A.; Composto, R. J. Experiments and Simulations Probing Local Domain Bulge and String Assembly of Aligned Nanoplates in a Lamellar Diblock Copolymer. *Macromolecules* **2019**, *52*, 8989−8999.
(173) Gao, W.; Sattayasamitsathit, S.; Manesh, K. M.; Weihs, D.; Wang, J. Magnetically powered flexible metal nanowire motors. *J. Am. Chem. Soc.* **2010**, *132*, 14403−14405.
(174) Wu, Z.; Lin, X.; Zou, X.; Sun, J.; He, Q. Biodegradable protein-based rockets for drug transportation and light-triggered release. *ACS Appl. Mater. Interfaces* **2015**, *7*, 250−255.
(175) Fan, D. L.; Cammarata, R. C.; Chien, C. L. Precision transport and assembling of nanowires in suspension by electric fields. *Appl. Phys. Lett.* **2008**, *92*, 093115.
(176) Wu, Z.; Si, T.; Gao, W.; Lin, X.; Wang, J.; He, Q. Superfast Near-Infrared Light-Driven Polymer Multilayer Rockets. *Small* **2016**, *12*, 577−582.
(177) Díez, P.; Esteban-Fernández De Ávila, B.; Ramírez-Herrera, D. E.; Villalonga, R.; Wang, J. Biomedical nanomotors: Efficient glucose-mediated insulin release. *Nanoscale* **2017**, *9*, 14307−14311.
(178) Hansen-Bruhn, M.; de Ávila, B. E. F.; Beltrán-Gastélum, M.; Zhao, J.; Ramírez-Herrera, D. E.; Angsantikul, P.; Vesterager Gothelf, K.; Zhang, L.; Wang, J. Active Intracellular Delivery of a Cas9/sgRNA Complex Using Ultrasound-Propelled Nanomotors. *Angewandte Chemie - International Edition* **2018**, *57*, 2657−2661.
(179) Wang, Y.; Hernandez, R. M.; Bartlett, D. J.; Bingham, J. M.; Kline, T. R.; Sen, A.; Mallouk, T. E. Bipolar electrochemical mechanism for the propulsion of catalytic nanomotors in hydrogen peroxide solutions. *Langmuir* **2006**, *22*, 10451−10456.
(180) Kagan, D.; Laocharoensuk, R.; Zimmerman, M.; Clawson, C.; Balasubramanian, S.; Kang, D.; Bishop, D.; Sattayasamitsathit, S.; Zhang, L.; Wang, J. Rapid delivery of drug carriers propelled and navigated by catalytic nanoshuttles. *Small* **2010**, *6*, 2741−2747.
(181) Gao, W.; Uygun, A.; Wang, J. Hydrogen-bubble-propelled zinc-based microrockets in strongly acidic media. *J. Am. Chem. Soc.* **2012**, *134*, 897−900.
(182) Manjare, M.; Yang, B.; Zhao, Y. P. Bubble-propelled microjets: Model and experiment. *J. Phys. Chem. C* **2013**, *117*, 4657−4665.
(183) Ma, X.; Hortelao, A. C.; Miguel-López, A.; Sánchez, S. Bubble-Free Propulsion of Ultrasmall Tubular Nanojets Powered by Biocatalytic Reactions. *J. Am. Chem. Soc.* **2016**, *138*, 13782−13785.
(184) Huang, Z.; Chen, P.; Zhu, G.; Yang, Y.; Xu, Z.; Yan, L.-T. Bacteria-Activated Janus Particles Driven by Chemotaxis. *ACS Nano* **2018**, *12*, 6725−6733.
(185) Deblais, A.; Woutersen, S.; Bonn, D. Rheology of Entangled Active Polymer-Like T. Tubifex Worms. *Phys. Rev. Lett.* **2020**, *124*, 188002.
(186) Amblard, F.; Maggs, A. C.; Yurke, B.; Pargellis, A. N.; Leibler, S. Subdiffusion and Anomalous Local Viscoelasticity in Actin Networks. *Phys. Rev. Lett.* **1996**, *77*, 4470.
(187) Tassieri, M.; Gibson, G. M.; Evans, R. M.; Yao, A. M.; Warren, R.; Padgett, M. J.; Cooper, J. M. Measuring storage and loss moduli using optical tweezers: Broadband microrheology. *Phys. Rev. E* **2010**, *81*, 1−5.
(188) Guo, M.; Ehrlicher, A. J.; Jensen, M. H.; Renz, M.; Moore, J. R.; Goldman, R. D.; Lippincott-Schwartz, J.; Mackintosh, F. C.; Weitz, D. A. Probing the stochastic, motor-driven properties of the cytoplasm using force spectrum microscopy. *Cell* **2014**, *158*, 822−832.
(189) Rigato, A.; Miyagi, A.; Scheuring, S.; Rico, F. High-frequency microrheology reveals cytoskeleton dynamics in living cells. *Nat. Phys.* **2017**, *13*, 771−775.
(190) Mandal, S.; Kurzthaler, C.; Franosch, T.; Löwen, H. Crowding-Enhanced Diffusion: An Exact Theory for Highly Entangled Self-Propelled Stiff Filaments. *Phys. Rev. Lett.* **2020**, *125*, 138002.
(191) Parisi, D.; Costanzo, S.; Jeong, Y.; Ahn, J.; Chang, T.; Vlassopoulos, D.; Halverson, J. D.; Kremer, K.; Ge, T.; Rubinstein, M.; Grest, G. S.; Srinin, W.; Grosberg, A. Y. Nonlinear Shear Rheology of Entangled Polymer Rings. *Macromolecules* **2021**, *54*, 2811−2827.
(192) Xu, Z.; Sun, R.; Lu, W.; Patil, S.; Mays, J.; Schweizer, K. S.; Cheng, S. Nature of Steady-State Fast Flow in Entangled Polymer

https://doi.org/10.1021/acs.macromol.3c00260
Macromolecules 2023, 56, 3809−3837

Melts: Chain Stretching, Shear Thinning, and Viscosity Scaling. *Macromolecules* **2022**, *55*, 10737−10750.
(193) Mei, B.; Lin, T. W.; Sheridan, G. S.; Evans, C. M.; Sing, C. E.; Schweizer, K. S. How Segmental Dynamics and Mesh Confinement Determine the Selective Diffusivity of Molecules in Cross-Linked Dense Polymer Networks. *ACS Cent. Sci.* **2023**, *9*, 508.
(194) Danielsen, S. P.; et al. Molecular Characterization of Polymer Networks. *Chem. Rev.* **2021**, *121*, 5042−5092.
(195) Xu, Z.; Dai, X.; Bu, X.; Yang, Y.; Zhang, X.; Man, X.; Zhang, X.; Doi, M.; Yan, L. T. Enhanced Heterogeneous Diffusion of Nanoparticles in Semiflexible Networks. *ACS Nano* **2021**, *15*, 4608−4616.
(196) Parrish, E.; Rose, K. A.; Cargnello, M.; Murray, C. B.; Lee, D.; Composto, R. J. Nanoparticle diffusion during gelation of tetra poly(ethylene glycol) provides insight into nanoscale structural evolution. *Soft Matter* **2020**, *16*, 2256−2265.
(197) Rose, K. A.; Lee, D.; Composto, R. J. pH-Mediated nanoparticle dynamics in hydrogel nanocomposites. *Soft Matter* **2021**, *17*, 2765−2774.
(198) Rose, K. A.; Marino, E.; O'Bryan, C. S.; Murray, C. B.; Lee, D.; Composto, R. J. Nanoparticle dynamics in hydrogel networks with controlled defects. *Soft Matter* **2022**, *18*, 9045−9056.
(199) Rose, K. A.; Gogotsi, N.; Galarraga, J. H.; Burdick, J. A.; Murray, C. B.; Lee, D.; Composto, R. J. Shape Anisotropy Enhances Nanoparticle Dynamics in Nearly Homogeneous Hydrogels. *Macromolecules* **2022**, *55*, 8514−8523.
(200) Schiller, J. L.; Lai, S. K. Tuning Barrier Properties of Biological Hydrogels. *ACS Applied Bio Materials* **2020**, *3*, 2875−2890.
(201) Lenzini, S.; Bargi, R.; Chung, G.; Shin, J. W. Matrix mechanics and water permeation regulate extracellular vesicle transport. *Nat. Nanotechnol.* **2020**, *15*, 217−223.
(202) Dobrynin, A. V. Polyelectrolytes: On the doorsteps of the second century. *Polymer* **2020**, *202*, 122714.
(203) Rumyantsev, A. M.; Borisov, O. V.; de Pablo, J. J. Structure and Dynamics of Hybrid Colloid-Polyelectrolyte Coacervates. *Macromolecules* **2023**, *56*, 1713−1730.
(204) Yamamoto, U.; Schweizer, K. S. Theory of nanoparticle diffusion in unentangled and entangled polymer melts. *J. Chem. Phys.* **2011**, *135*, 224902.
(205) Yamamoto, U.; Schweizer, K. S. Spatially dependent relative diffusion of nanoparticles in polymer melts. *J. Chem. Phys.* **2013**, *139*, 064907.
(206) Ge, T.; Cheng, S. Physicochemical properties of respiratory droplets and their role in COVID-19 pandemics: a critical review. *Biomate. Transl.* **2021**, *2*, 10−18.

https://doi.org/10.1021/acs.macromol.3c00260
Macromolecules 2023, 56, 3809−3837